INTERNATIONAL JOURNAL FOR NUMERICAL METHODS IN FLUIDS
Int. J. Numer. Meth. Fluids 2003; **41**:77–107 (DOI: 10.1002/fld.426)

Topology optimization of fluids in Stokes flow

Thomas Borrvall*,† and Joakim Petersson

Division of Mechanics, Mechanical Engineering Systems, Linköping University, SE-581 83 Linköping, Sweden

SUMMARY

We consider topology optimization of fluids in Stokes flow. The design objective is to minimize a power function, which for the absence of body fluid forces is the dissipated power in the fluid, subject to a fluid volume constraint. A generalized Stokes problem is derived that is used as a base for introducing the design parameterization. Mathematical proofs of existence of optimal solutions and convergence of discretized solutions are given and it is concluded that no regularization of the optimization problem is needed. The discretized state problem is a mixed finite element problem that is solved by a pre-conditioned conjugate gradient method and the design optimization problem is solved using sequential separable and convex programming. Several numerical examples are presented that illustrate this new methodology and the results are compared to results obtained in the context of shape optimization of fluids. Copyright © 2003 John Wiley & Sons, Ltd.

1. INTRODUCTION

Shape optimization in fluid mechanics is an active research field since several decades. The desired achievements have for instance been to obtain minimum drag wing profiles [1–5] and minimum pressure drop diffusers [6]. When striving for a decreased drag or pressure drop, the feasible design modifications have concerned adjusting selected parts of the boundary to the fluid region. In *topology* optimization the goal is to not only modify boundary shapes but also to allow for new boundaries to appear as part of the solution to the optimization problem, hence allowing for a change in connectedness of the fluid region. This kind of optimization is well established within mechanics of solids and structures where the amount of work is abundant, see References [7, 8] for an overview. However, to the authors' knowledge, the methodology has not previously been applied to optimal design in *fluid* mechanics.

* Correspondence to: T. Borrvall, Engineering Research Nordic AB, Garnisonen, Brigadgatan 16, SE-581 31 Linköping, Sweden.
† E-mail: thomas.borrvall@erab.se

Contract/grant sponsor: National Graduate School in Scientific Computing
Contract/grant sponsor: National Network in Applied Mathematics
Contract/grant sponsor: Swedish Research Council
Contract/grant sponsor: Centre for Industrial Information Technology

Received 1 February 2002
Accepted 16 August 2002

In the present work a direction of research is suggested and initiated where these developments are done for continuum fluid mechanics. A similar treatment for discrete Poiseuille flow networks is given in Reference [9].

Given a predetermined design domain Ω with certain boundary conditions, the goal is to determine at what places of Ω there should be fluid and where there should be nonfluid (i.e. solid), in order to minimize a certain power subject to a given amount of fluid. We consider creeping flows of Newtonian fluids, i.e. Stokes flows, and the objective reduces to minimizing drag or pressure drop in special cases. This setup should allow for possible new applications in design of minimum head loss valves, models in biofluid mechanics, and other applications in process industries and microfluidics.

In topology optimization in continuum physics the design parameterization often ends up with a scaling of some constitutive parameter E while keeping the domain Ω fixed. One introduces a design function ρ which ultimately should be the characteristic function for the optimal distribution of the medium in which the 'physical process' is taking place. The constitutive parameter E is taken to be a function of ρ in such a way that intermediate values of ρ, i.e. values between zero and one, are feasible but somehow penalized. When the physical process is represented by linear elasticity, governed by the Cauchy–Navier's system of equations, $E(\rho)$ is the Young's modulus where the parameterization is such that $E(0) \approx 0$ to model a hole and $E(1) = E_0$ to model presence of material with modulus E_0, cf. Reference [10]. Almost identically one can parameterize the conductivity in static heat transfer, governed by the Poisson's equation.

In this work we are using the generalized Stokes partial differential equation [11] to represent the physical process, i.e. to determine the flow velocity $\boldsymbol{u}$ and pressure p. This equation involves the elliptic operator $\alpha I - \mu\Delta$ in which μ is the viscosity and α can be called inverse permeability. When $\alpha = 0$ one retains Stokes flow with viscosity μ and when $\mu = 0$ one gets the Darcy equation that governs porous media flow with permeability α^{-1}. The scalar α also appears when solving a subproblem in the time-dependent Navier–Stokes equations [12].

The design parameterization is in this paper performed such that the viscosity is kept constant whereas the permeability α^{-1} depends on ρ in such a way that it is very small at nonfluid places and very large to recover Stokes flow at fluid places. Hence, we are not scaling the viscosity but rather introducing a kind of penalty factor α on the velocities $\boldsymbol{u}$ such that $\alpha(0)$ is very large and $\alpha(1)$ is very small. Subsequently we motivate this design parameterization by deriving a plane flow model in Couette flow. Here, a two-dimensional generalized Stokes model with $\alpha(\rho) = 2.5\mu/\rho^2$ is derived starting from a Stokes three-dimensional model (with no α present). The parameter ρ is then half the thickness of the layer in which the three-dimensional Stokes flow with constant viscosity μ is taking place.

The analyses are then carried out for a general decreasing, convex and continuously differentiable design parameterization $\rho \mapsto \alpha(\rho)$, and all methodologies are valid in both two and three dimensions. We prove existence of optimal designs for such general $\rho \mapsto \alpha(\rho)$, and for the special case of linear $\rho \mapsto \alpha(\rho)$ there exist optimal ρ:s that are completely discrete-valued, i.e. the problem is 'fully penalized'. These are quite unexpected results since it is atypical for the situation in solids' topology optimization. For elastic continua the optimal design problem typically lacks solutions. This can be understood by considering the fact that the objective function, like structural stiffness, can be improved on by splitting up solid parts into several thinner parts (without changing the volume). To cure this, the problem is regularized by either expanding the set of feasible designs or by restricting it. The latter can be performed

by enforcing a constraint on e.g. the perimeter of the domain, and the former means to allow variable microstructure which is handled by using homogenization. The typical goal of minimizing the dissipation power in Stokes flow does *not* require finer scale for the fluid parts: Replacing one pipe with a prescribed flow with two pipes of half the width, which together deliver the same flow, gives twice as large dissipation power.

Hence the situation is different from the ones in solids. Performing homogenization in the linear elasticity equations, one retains the same equations. If one introduces rigid balls with diameter ε in fluids in Stokes flow, however, then the velocity $\boldsymbol{u}^\varepsilon$ converges to zero, but $\boldsymbol{u}^\varepsilon/\varepsilon^2$ converges to $\boldsymbol{u}$ which is part of the solution to the Darcy problem (in which the permeability tensor is related in a specific way to the Stokes problem data) [13]. This means, first, that the flow becomes worse, not better, (in the sense of the objective function) as one performs the homogenization process, and, secondly, the process converges (after a rescaling by ε^2), to a different state equation. Concluding, on the one hand, the homogenization process is not needed in Stokes flow topology optimization since existence of optimal designs can be guaranteed without any regularization, but, on the other hand, this process introduces a permeability of porous media which we have included in parallel with the viscosity of Stokes flows.

The rest of the paper is organized as follows. In Section 2, we present the generalized Stokes system that is used as a constraint in the design optimization problem. This equation is derived from a three-dimensional conventional Stokes system under a certain plane flow assumption. The section ends with a thorough treatment of how this state problem is solved numerically. A mixed finite element formulation is used and the resulting system of equations is solved efficiently by a preconditioned conjugate gradient method. Section 3 is devoted to the design optimization problem, stated as to minimize a power function subject to a fluid volume constraint, including presentations of the continuum as well as finite element discretized formulations. Rigorous mathematical proofs of existence of solutions and convergence of the finite element schemes are presented. Regarding the numerical solution of this optimization problem, we use sequential separable and convex programming, a solution method that is frequently used in the context of topology optimization of solids. In Section 4, several numerical examples are presented that illustrate this new methodology. The examples are commented upon and when possible, compared to well-known fluid shape optimization results. The paper ends with some discussion and conclusions in Section 5.

2. THE STATE PROBLEM

2.1. Continuum mechanical background

We give the needed background from continuum mechanics, following mainly [14].

Consider the flow of an incompressible, Newtonian fluid with constant viscosity μ in the control volume $\mathscr{R} \subset \boldsymbol{R}^3$. The constitutive equation expressing the Cauchy stress $\boldsymbol{T}$ in terms of pressure $\bar{p}$ and flow velocity $\bar{\boldsymbol{u}}$ is then

$$\boldsymbol{T} = -\bar{p}\boldsymbol{I} + 2\mu \boldsymbol{D}(\bar{\boldsymbol{u}}) \tag{1}$$

where the rate-of-strain tensor $\boldsymbol{D}(\bar{\boldsymbol{u}})$ is given by

$$\boldsymbol{D}(\bar{\boldsymbol{u}}) = \frac{1}{2}(\nabla \bar{\boldsymbol{u}} + (\nabla \bar{\boldsymbol{u}})^{\mathrm{T}}) \tag{2}$$

with ∇ denoting the spatial gradient. The equation of motion reads

$$\rho_0 \left(\frac{\partial \bar{\boldsymbol{u}}}{\partial t} + (\nabla \bar{\boldsymbol{u}})\bar{\boldsymbol{u}} \right) = \operatorname{div} \boldsymbol{T} + \bar{\boldsymbol{f}} \tag{3}$$

where ρ_0, $\bar{\boldsymbol{f}}$ are the reference density and body force, respectively, and $\partial/\partial t$, div the spatial time derivative and divergence, respectively. Together with the incompressibility condition $\operatorname{div} \bar{\boldsymbol{u}} = 0$ the constitutive equation (1) into the equation of motion (3) results in the Navier–Stokes equations

$$\rho_0 \left(\frac{\partial \bar{\boldsymbol{u}}}{\partial t} + (\nabla \bar{\boldsymbol{u}})\bar{\boldsymbol{u}} \right) = \operatorname{div}(2\mu \boldsymbol{D}(\bar{\boldsymbol{u}})) - \nabla \bar{p} + \bar{\boldsymbol{f}}$$

$$\operatorname{div} \bar{\boldsymbol{u}} = 0$$

Using the incompressibility condition and the fact that μ is constant, these can be written as

$$\begin{aligned} \rho_0 \left(\frac{\partial \bar{\boldsymbol{u}}}{\partial t} + (\nabla \bar{\boldsymbol{u}})\bar{\boldsymbol{u}} \right) &= \mu \Delta \bar{\boldsymbol{u}} - \nabla \bar{p} + \bar{\boldsymbol{f}} \\ \operatorname{div} \bar{\boldsymbol{u}} &= 0 \end{aligned} \tag{4}$$

For slow and steady flow, the convection term $(\nabla \bar{\boldsymbol{u}})\bar{\boldsymbol{u}}$ is neglected and the spatial time derivative $\partial \bar{\boldsymbol{u}}/\partial t$ vanishes. The Navier–Stokes equations (4) then reduce to the Stokes equations

$$\begin{aligned} \mu \Delta \bar{\boldsymbol{u}} &= \nabla \bar{p} - \bar{\boldsymbol{f}} \\ \operatorname{div} \bar{\boldsymbol{u}} &= 0 \end{aligned} \tag{5}$$

In general we assume that the velocity $\bar{\boldsymbol{u}}$ is prescribed to some known function $\bar{\boldsymbol{g}}$ on $\partial \mathscr{R}$. By integrating the incompressibility condition over $\mathscr{R}$ and using the divergence theorem it is easy to see that the function $\bar{\boldsymbol{g}}$ must satisfy the following compatibility condition:

$$\int_{\partial \mathscr{R}} \bar{\boldsymbol{g}} \cdot \boldsymbol{n} = 0 \tag{6}$$

where $\boldsymbol{n}$ denotes the outward unit normal. Some further continuum mechanical arguments, needed for an alternative interpretation of the design objective to be treated, are given in the appendix.

2.2. *Variational formulation*

Let $\bar{\boldsymbol{v}}$ be any velocity function which is zero on the boundary to the control volume, $\partial \mathscr{R}$. Multiplying the first of (5) by $\bar{\boldsymbol{v}}$ and integrating over $\mathscr{R}$ one obtains the equation of virtual power,

$$\mu \int_{\mathscr{R}} \nabla \bar{\boldsymbol{u}} \cdot \nabla \bar{\boldsymbol{v}} - \int_{\mathscr{R}} \bar{p} \operatorname{div} \bar{\boldsymbol{v}} = \int_{\mathscr{R}} \bar{\boldsymbol{f}} \cdot \bar{\boldsymbol{v}} \tag{7}$$

after having used the Green's theorem. With the dissipation power bilinear form

$$A(\bar{\boldsymbol{u}}, \bar{\boldsymbol{v}}) = \mu \int_{\mathscr{R}} \nabla \bar{\boldsymbol{u}} \cdot \nabla \bar{\boldsymbol{v}}$$

and the functionals

$$B(\bar{\boldsymbol{v}}, \bar{p}) = -\int_{\mathscr{R}} \bar{p} \operatorname{div} \bar{\boldsymbol{v}}, \quad \langle \bar{\boldsymbol{f}}, \bar{\boldsymbol{v}} \rangle_{\mathscr{R}} = \int_{\mathscr{R}} \bar{\boldsymbol{f}} \cdot \bar{\boldsymbol{v}}$$

the equation of virtual power (7) can be compactly written as

$$A(\bar{\boldsymbol{u}}, \bar{\boldsymbol{v}}) + B(\bar{\boldsymbol{v}}, \bar{p}) = \langle \bar{\boldsymbol{f}}, \bar{\boldsymbol{v}} \rangle_{\mathscr{R}} \tag{8}$$

The second of (5) multiplied by any pressure function $\bar{q}$ and integrated over $\mathscr{R}$ is

$$B(\bar{\boldsymbol{u}}, \bar{q}) = 0 \tag{9}$$

Equations (8) and (9) will appear in the weak formulation (10) of the Stokes problem, which can be posed after some function spaces have been introduced; define

$$\bar{\Pi} = L_0^2(\mathscr{R}) = \left\{ \bar{q} \in L^2(\mathscr{R}) \,\middle|\, \int_{\mathscr{R}} \bar{q} = 0 \right\}$$

for pressure functions, and

$$\bar{\boldsymbol{V}} = \boldsymbol{H}_0^1(\mathscr{R}) = \{ \bar{\boldsymbol{v}} \in \boldsymbol{H}^1(\mathscr{R}) \,|\, \bar{\boldsymbol{v}} = \boldsymbol{0} \text{ on } \partial\mathscr{R} \}$$
$$\bar{\boldsymbol{U}} = \{ \bar{\boldsymbol{v}} \in \boldsymbol{H}^1(\mathscr{R}) \,|\, \bar{\boldsymbol{v}} = \bar{\boldsymbol{g}} \text{ on } \partial\mathscr{R} \}$$

for velocity functions. Furthermore, we assume that $\bar{\boldsymbol{g}} \in \boldsymbol{H}^{1/2}(\partial\mathscr{R})$ and $\bar{\boldsymbol{f}} \in \boldsymbol{L}^2(\mathscr{R})$. The weak form of Stokes problem (5) can be formulated as follows: Find $(\bar{\boldsymbol{u}}, \bar{p}) \in \bar{\boldsymbol{U}} \times \bar{\Pi}$ such that

$$\begin{aligned} A(\bar{\boldsymbol{u}}, \bar{\boldsymbol{v}}) + B(\bar{\boldsymbol{v}}, \bar{p}) &= \langle \bar{\boldsymbol{f}}, \bar{\boldsymbol{v}} \rangle_{\mathscr{R}} \quad \forall \bar{\boldsymbol{v}} \in \bar{\boldsymbol{V}} \\ B(\bar{\boldsymbol{u}}, \bar{q}) &= 0 \qquad\qquad \forall \bar{q} \in \bar{\Pi} \end{aligned} \tag{10}$$

If $\mathscr{R}$ is open, bounded and connected with a Lipschitz continuous boundary $\partial\mathscr{R}$, the Stokes problem (10) is uniquely solvable, see for instance Reference [15].

2.3. A plane flow model

Consider a domain $\mathscr{R} \subset \boldsymbol{R}^3$ that is essentially plane, see Figure 1 for an illustration. That is, $\mathscr{R}$ is the cartesian product of a bounded domain $\Omega \subset \boldsymbol{R}^2$ and a short interval $[-\rho, \rho]$,

$$\mathscr{R} = \{ \boldsymbol{x} = (x_1, x_2, x_3) \in \boldsymbol{R}^3 \,|\, (x_1, x_2) \in \Omega, \quad -\rho \leqslant x_3 \leqslant \rho \}$$

To start with we assume that ρ is a small positive constant and introduce the scalar function $\xi : \mathscr{R} \to \boldsymbol{R}$ given by

$$\xi(\boldsymbol{x}) = \xi(x_1, x_2, x_3) = 1 - \left(\frac{x_3}{\rho} \right)^2$$

The boundary function $\bar{\boldsymbol{g}}$ and external body fluid force field $\bar{\boldsymbol{f}}$ are assumed on the following form

$$\begin{aligned} \bar{\boldsymbol{g}} &= \xi \boldsymbol{g} \\ \bar{\boldsymbol{f}} &= \xi \boldsymbol{f} \end{aligned} \tag{11}$$

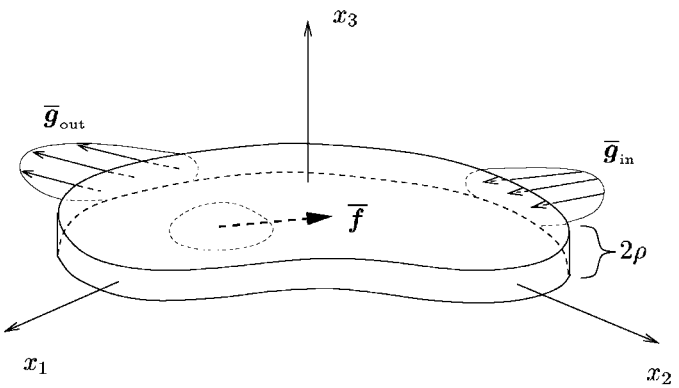

Figure 1. Illustration of a plane flow model.

where $\boldsymbol{g} \in \boldsymbol{H}^{1/2}(\partial\Omega)$ and $\boldsymbol{f} \in \boldsymbol{L}^2(\Omega)$ respectively. For $\boldsymbol{g}$ constant and $\boldsymbol{f} = \boldsymbol{0}$, i.e., no body fluid forces, the velocity solution to the Stokes equations (10) is

$$\bar{\boldsymbol{u}} = \xi \boldsymbol{g}$$

The pressure solution can be determined from

$$\nabla \bar{p} = -\frac{2\mu}{\rho^2}\boldsymbol{g}$$

meaning that $\bar{p}$ is an affine function that is independent of x_3. This is in the literature known as Couette flow, flow between two parallel surfaces. Knowing the solution in this special case and that ρ is small, we assume that for data as in (11), the solution to Stokes equations (11) is contained in the closed subset $\bar{\boldsymbol{U}}_{\|} \times \bar{\Pi}_{\|} \subset \bar{\boldsymbol{U}} \times \bar{\Pi}$ defined by

$$\bar{\boldsymbol{U}}_{\|} = \{\bar{\boldsymbol{v}} \in \bar{\boldsymbol{U}} \mid \bar{\boldsymbol{v}} = \xi \boldsymbol{v}, \quad \boldsymbol{v} \in \boldsymbol{U}\}$$

$$\bar{\Pi}_{\|} = \{\bar{q} \in \bar{\Pi} \mid \bar{q} = \tfrac{4}{5} q, \quad q \in \Pi\}$$

where

$$\boldsymbol{U} = \{\boldsymbol{v} \in \boldsymbol{H}^1(\Omega) \mid \boldsymbol{v} = \boldsymbol{g} \text{ on } \partial\Omega\}$$

$$\Pi = L_0^2(\Omega) = \left\{ q \in L^2(\Omega) \mid \int_\Omega q = 0 \right\}$$

The space of test functions corresponding to $\bar{\boldsymbol{U}}_{\|}$ is

$$\bar{\boldsymbol{V}}_{\|} = \{\bar{\boldsymbol{v}} \in \bar{\boldsymbol{V}} \mid \bar{\boldsymbol{v}} = \xi \boldsymbol{v}, \quad \boldsymbol{v} \in \boldsymbol{V}\}$$

where

$$\boldsymbol{V} = \boldsymbol{H}_0^1(\Omega) = \{\boldsymbol{v} \in \boldsymbol{H}^1(\Omega) \mid \boldsymbol{v} = \boldsymbol{0} \text{ on } \partial\Omega\}$$

The solution that we are looking for is given by the solution to (10) with $\bar{\boldsymbol{U}}$, $\bar{\boldsymbol{V}}$ and $\bar{\Pi}$ substituted for $\bar{\boldsymbol{U}}_{\|}$, $\bar{\boldsymbol{V}}_{\|}$ and $\bar{\Pi}_{\|}$: Find $(\bar{\boldsymbol{u}}, \bar{p}) \in \bar{\boldsymbol{U}}_{\|} \times \bar{\Pi}_{\|}$ such that

$$\begin{aligned} A(\bar{\boldsymbol{u}}, \bar{\boldsymbol{v}}) + B(\bar{\boldsymbol{v}}, \bar{p}) &= \langle \bar{\boldsymbol{f}}, \bar{\boldsymbol{v}} \rangle_{\mathscr{R}} \quad \forall \bar{\boldsymbol{v}} \in \bar{\boldsymbol{V}}_{\|} \\ B(\bar{\boldsymbol{u}}, \bar{q}) &= 0 \qquad\qquad \forall \bar{q} \in \bar{\Pi}_{\|} \end{aligned}$$

Here ξ is the only component that depends on x_3 and straightforward calculation shows that this problem is equivalent to: Find $(\boldsymbol{u}, p) \in \boldsymbol{U} \times \Pi$ so that

$$\begin{aligned} a_{\alpha}(\boldsymbol{u}, \boldsymbol{v}) + b(\boldsymbol{v}, p) &= \langle \boldsymbol{f}, \boldsymbol{v} \rangle \quad \forall \boldsymbol{v} \in \boldsymbol{V} \\ b(\boldsymbol{u}, q) &= 0 \qquad\quad \forall q \in \Pi \end{aligned} \tag{12}$$

with

$$\begin{aligned} a_{\alpha}(\boldsymbol{u}, \boldsymbol{v}) &= \int_{\Omega} \alpha(\rho) \boldsymbol{u} \cdot \boldsymbol{v} + \mu \int_{\Omega} \nabla \boldsymbol{u} \cdot \nabla \boldsymbol{v} \\ \alpha(\rho) &= \frac{5\mu}{2\rho^2} \\ b(\boldsymbol{v}, p) &= -\int_{\Omega} p \operatorname{div} \boldsymbol{v} \\ \langle \boldsymbol{f}, \boldsymbol{v} \rangle &= \int_{\Omega} \boldsymbol{f} \cdot \boldsymbol{v} \end{aligned} \tag{13}$$

Problem (12) is a *generalized Stokes problem* which for instance appears as a subproblem when solving the time-dependent Navier–Stokes equations (4), see Reference [12]. The three-dimensional solution $(\bar{\boldsymbol{u}}, \bar{p})$ can be retained by multiplying $\boldsymbol{u}$ by ξ and p by $4/5$ as indicated in the definitions of $\bar{\boldsymbol{U}}_{\|}$ and $\bar{\Pi}_{\|}$. As for the Stokes equations (10), (12) is uniquely solvable if only Ω is open, bounded and connected with a Lipschitz continuous boundary $\partial\Omega$.

Define the total potential power function $\mathscr{J}_{\alpha} : \boldsymbol{H}^1(\Omega) \to \boldsymbol{R}$ by

$$\mathscr{J}_{\alpha}(\boldsymbol{v}) = \tfrac{1}{2} a_{\alpha}(\boldsymbol{v}, \boldsymbol{v}) - \langle \boldsymbol{f}, \boldsymbol{v} \rangle \tag{14}$$

and the following closed subset of $\boldsymbol{U}$:

$$\boldsymbol{U}_{\mathrm{div}} = \{ \boldsymbol{v} \in \boldsymbol{U} \mid \operatorname{div} \boldsymbol{v} = 0 \}$$

Then the velocity that solves (12) can be found by minimizing the total potential power over all velocities in $\boldsymbol{U}_{\mathrm{div}}$, i.e.

$$\mathscr{J}_{\alpha}(\boldsymbol{u}) = \min_{\boldsymbol{v} \in \boldsymbol{U}_{\mathrm{div}}} \mathscr{J}_{\alpha}(\boldsymbol{v})$$

The stationarity condition for this convex minimization problem is exactly (12). To see this, relax the constraint $\operatorname{div} \boldsymbol{v} = 0$ and form the Lagrangian

$$\mathscr{L}_{\alpha}(\boldsymbol{v}, q) = \mathscr{J}_{\alpha}(\boldsymbol{v}) + b(\boldsymbol{v}, q)$$

and look for a saddle point over all $(\boldsymbol{v}, q) \in \boldsymbol{U} \times \Pi$. The saddle point $(\boldsymbol{u}, p) \in \boldsymbol{U} \times \Pi$ then satisfies (12).

To summarize, by making suitable assumptions we have reduced a three-dimensional problem (10) to a two-dimensional problem (12). The dissipated power due to out-of-plane shears in (10) is in (12) modelled by an absorption term involving the inverse of a permeability factor, α. A corresponding term involving the permeability tensor appears in Darcy's law when homogenizing the Stokes equations, see Reference [13]. A crucial difference is that (12) includes a classical Stokes term modelling the dissipated power due to in-plane shears that is not present in Darcy's law. This means that we can here retain the two-dimensional Stokes equations by putting $\alpha = 0$ (or $\rho = \infty$).

At this point we allow ρ to vary in space. The generalized Stokes problem (12) with the function α given by the second of (13) governs the flow between two nonplane surfaces separated by a distance determined by the function ρ. The interpretation of α above suggests that ρ could be used as a design variable in the context of topology optimization since the permeability is increasing in ρ. We will discuss this idea in more detail in Section 3 where an optimization problem is presented in which an optimal density of fluid is sought for.

2.4. Finite element discretization

We now turn our attention to the problem of finding finite element approximations to the functions $\boldsymbol{u}$ and p given by the solution to (12) in the previous section. To this end, we assume that Ω is discretized into finite elements with h denoting a characteristic size of the largest element. With respect to this mesh, the finite dimensional approximation spaces $\Pi_h \subset \Pi$, $\boldsymbol{W}_h \subset \boldsymbol{H}^1(\Omega)$ and, as a consequence, $\boldsymbol{V}_h = \boldsymbol{W}_h \cap \boldsymbol{V}$ are constructed. The exact details on how these spaces, as well as how the mesh, are constructed are given later on in this section. Let $\tilde{\boldsymbol{g}}_h \in \boldsymbol{W}_h$ be so that $\boldsymbol{g}_h = \mathrm{Tr}(\tilde{\boldsymbol{g}}_h)$ is a suitable approximation of the prescribed boundary function $\boldsymbol{g}$. The approximation of $\boldsymbol{U}$ is given by

$$\boldsymbol{U}_h = \{\boldsymbol{v}_h \in \boldsymbol{W}_h \mid \boldsymbol{v}_h = \boldsymbol{g}_h \text{ on } \partial\Omega\}$$

The finite element discretized problem that corresponds to problem (12) reads: Find $(\boldsymbol{u}_h, p_h) \in \boldsymbol{U}_h \times \Pi_h$ such that

$$\begin{aligned} a_\alpha(\boldsymbol{u}_h, \boldsymbol{v}_h) + b(\boldsymbol{v}_h, p_h) &= \langle \boldsymbol{f}, \boldsymbol{v}_h \rangle \quad \forall \boldsymbol{v}_h \in \boldsymbol{V}_h \\ b(\boldsymbol{u}_h, q_h) &= 0 \qquad\quad \forall q_h \in \Pi_h \end{aligned} \tag{15}$$

By putting $\boldsymbol{u}_h = \boldsymbol{u}_h^0 + \tilde{\boldsymbol{g}}_h$, this problem can be rephrased as to: Find $(\boldsymbol{u}_h^0, p_h) \in \boldsymbol{V}_h \times \Pi_h$ such that

$$\begin{aligned} a_\alpha(\boldsymbol{u}_h^0, \boldsymbol{v}_h) + b(\boldsymbol{v}_h, p_h) &= \langle \boldsymbol{f}, \boldsymbol{v}_h \rangle - a_\alpha(\tilde{\boldsymbol{g}}_h, \boldsymbol{v}_h) \quad \forall \boldsymbol{v}_h \in \boldsymbol{V}_h \\ b(\boldsymbol{u}_h^0, q_h) &= -b(\tilde{\boldsymbol{g}}_h, q_h) \qquad\qquad\quad \forall q_h \in \Pi_h \end{aligned} \tag{16}$$

which is a mixed finite element problem that we intend to solve.

The construction of the space $\boldsymbol{W}_h$ is merely a question of approximation theory, meaning that the space $\boldsymbol{W}_h$ should be 'close' to $\boldsymbol{H}^1(\Omega)$ measured in $\boldsymbol{H}^1(\Omega)$-norm. The space Π_h should not only have good approximation properties, but it cannot be too big as this would cause numerical instabilities such as for instance 'locking' phenomena and checkerboard-like tendencies. To assure numerical stability, the spaces $\boldsymbol{W}_h$ and Π_h should be constructed so that

$$\sup_{\boldsymbol{0} \neq \boldsymbol{v}_h \in \boldsymbol{V}_h} \frac{b(\boldsymbol{v}_h, q_h)}{\|\boldsymbol{v}_h\|_1} \geqslant \beta \|q_h\|_0 \quad \forall q_h \in \Pi_h \tag{17}$$

for some $\beta > 0$ independent of h. We have introduced $\|\cdot\|_1$ and $\|\cdot\|_0$ denoting any standard norm in $\boldsymbol{H}^1(\Omega)$ and $L^2(\Omega)$, respectively. Condition (17) is known as the discrete inf-sup condition or the Ladyszhenskaya–Babuška–Brezzi (LBB) condition and is a necessity for the convergence of $(\boldsymbol{u}_h, p_h)$ to $(\boldsymbol{u}, p)$. Once (17) is established, one has the following standard error estimate [16]:

$$\|\boldsymbol{u}_h - \boldsymbol{u}\|_1 + \|p_h - p\|_0 \leqslant C\left(\inf_{\boldsymbol{v}_h \in \boldsymbol{U}_h} \|\boldsymbol{v}_h - \boldsymbol{u}\|_1 + \inf_{q_h \in \Pi_h} \|q_h - p\|_0\right) \tag{18}$$

if the boundary velocity is conveniently approximated, or assuming $\boldsymbol{g}_h = \boldsymbol{g}$ for convenience. Hence, if the space Π_h approximates Π well in $L^2(\Omega)$-norm and $\boldsymbol{U}_h$ approximates $\boldsymbol{U}$ well in $\boldsymbol{H}^1(\Omega)$-norm, convergence is guaranteed.

In this context, an accurate and stable mixed finite element method is the Hood–Taylor method. In this method Ω is triangulated and the approximation spaces Π_h and $\boldsymbol{W}_h$ are chosen as the continuous functions that are piecewise linear and quadratic, respectively. Here we consider a popular variant of this method that is more suitable for the application we have in mind. In all our numerical examples, Ω is a rectangle and hence it is more convenient to use rectangular finite elements. Thus the domain is divided into $N_x \times N_y$ identical quadrilateral elements, called P-elements. The pressure space Π_h is the space of functions that are continuous and piecewise bilinear. To determine the velocity space $\boldsymbol{W}_h$, each P-element is further divided into 2×2 elements, resulting in a mesh of $2N_x \times 2N_y$ U-elements. The space $\boldsymbol{W}_h$ consists of the continuous functions that are bilinear in each U-element. Apart from using quadrilaterals instead of triangles, the difference between the Hood–Taylor method and the method used here is that piecewise quadratic velocity functions are substituted for piecewise (bi-)linear velocity functions while at the same time a finer velocity mesh is used to maintain stability. The reason for not using piecewise quadratic velocity functions is that the computational effort related to such functions is much higher compared to the resolution in the optimal design.

2.5. Matrix–vector formulations

Let $\mathbf{u}$ be the vector of all nodal velocity values for $\boldsymbol{u}_h$, including those on $\partial\Omega$. The matrices $\mathbf{C}_1$ and $\mathbf{C}_2$ give the vector of nodal displacement values on $\partial\Omega$, $\mathbf{u}_1$, and the vector of nodal displacements in the interior of Ω, $\mathbf{u}_2$, respectively;

$$\mathbf{C}_1\mathbf{u} = \mathbf{u}_1, \quad \mathbf{C}_2\mathbf{u} = \mathbf{u}_2$$

This decomposition is made so that

$$\mathbf{u} = \mathbf{C}_1^{\mathrm{T}}\mathbf{u}_1 + \mathbf{C}_2^{\mathrm{T}}\mathbf{u}_2 \tag{19}$$

the matrix $[\mathbf{C}_1^{\mathrm{T}}, \mathbf{C}_2^{\mathrm{T}}]^{\mathrm{T}}$ is invertible, and $\mathbf{C}_1\mathbf{C}_1^{\mathrm{T}}$ and $\mathbf{C}_2\mathbf{C}_2^{\mathrm{T}}$ are identity matrices (with some dimension). The body forces in the interior are represented by the load vector $\mathbf{F}$ which is work conjugate to $\mathbf{u}_2$, so the (virtual) work by the load (per unit time) is $\mathbf{F}^{\mathrm{T}}\mathbf{u}_2 = \mathbf{F}^{\mathrm{T}}\mathbf{C}_2\mathbf{u}$. The bilinear form gives a symmetric and positive semidefinite stiffness matrix $\tilde{\mathbf{K}}_\alpha$ which includes also the nodes on $\partial\Omega$. The matrix $\mathbf{B}$ denotes the discretized divergence operator and $\mathbf{B}^{\mathrm{T}}$ the discretized gradient operator, and $\mathbf{g}$ is the discretized boundary function $\boldsymbol{g}_h$ and $\tilde{\mathbf{g}} = \mathbf{C}_1^{\mathrm{T}}\mathbf{g}$ the vector version of $\tilde{\boldsymbol{g}}_h$. The discretized version of $\mathscr{J}_\alpha$ then becomes

$$J_\alpha(\mathbf{v}) = \tfrac{1}{2}\,\mathbf{v}^{\mathrm{T}}\tilde{\mathbf{K}}_\alpha\mathbf{v} - \mathbf{F}^{\mathrm{T}}\mathbf{C}_2\mathbf{v} \tag{20}$$

which should be minimized subject to incompressibility and inhomogeneous Dirichlet conditions,

$$\mathbf{B}\mathbf{v} = \mathbf{0}, \quad \mathbf{C}_1\mathbf{v} = \mathbf{g} \tag{21}$$

By using (19) and $\mathbf{C}_1^{\mathrm{T}}\mathbf{v}_1 = \tilde{\mathbf{g}}$, minimizing (20) subject to constraints (21) can be reduced to minimizing

$$\tilde{J}_\alpha(\mathbf{v}_2) = \tfrac{1}{2}\,\mathbf{v}_2^{\mathrm{T}}\mathbf{K}_\alpha\mathbf{v}_2 - (\mathbf{F} - \mathbf{C}_2\tilde{\mathbf{K}}_\alpha\tilde{\mathbf{g}})^{\mathrm{T}}\mathbf{v}_2 + \tfrac{1}{2}\,\tilde{\mathbf{g}}\tilde{\mathbf{K}}_\alpha\tilde{\mathbf{g}} \tag{22}$$

subject to the constraints

$$\mathbf{B}\mathbf{C}_2^{\mathrm{T}}\mathbf{v}_2 = -\mathbf{B}\tilde{\mathbf{g}} \tag{23}$$

Here the matrix $\mathbf{K}_\alpha = \mathbf{C}_2\tilde{\mathbf{K}}_\alpha\mathbf{C}_2^{\mathrm{T}}$ is the stiffness matrix including only the nodes in the interior of Ω. A vector $\mathbf{u}_2$ solves this quadratic program if and only if the Karush–Kuhn–Tucker conditions hold, cf. (16),

$$\begin{aligned} \mathbf{K}_\alpha\mathbf{u}_2 + \mathbf{C}_2\mathbf{B}^{\mathrm{T}}\mathbf{p} &= \mathbf{F} - \mathbf{C}_2\tilde{\mathbf{K}}_\alpha\tilde{\mathbf{g}} \\ \mathbf{B}\mathbf{C}_2^{\mathrm{T}}\mathbf{u}_2 &= -\mathbf{B}\tilde{\mathbf{g}} \end{aligned} \tag{24}$$

where $\mathbf{p}$ is the Lagrange multiplier for constraint (23), i.e. the discretized pressure. Since $\mathbf{K}_\alpha$ is positive definite, one can solve for $\mathbf{u}_2$ in the first of (24) and then plug this into the second of (24). One obtains the following equation system in pressure only:

$$\mathbf{H}_\alpha\mathbf{p} = \mathbf{h}_\alpha \tag{25}$$

where

$$\mathbf{H}_\alpha = \mathbf{B}\mathbf{C}_2^{\mathrm{T}}\mathbf{K}_\alpha^{-1}\mathbf{C}_2\mathbf{B}^{\mathrm{T}}, \quad \mathbf{h}_\alpha = \mathbf{B}\mathbf{C}_2^{\mathrm{T}}\mathbf{K}_\alpha^{-1}(\mathbf{F} - \mathbf{C}_2\tilde{\mathbf{K}}_\alpha\tilde{\mathbf{g}}) + \mathbf{B}\tilde{\mathbf{g}}$$

Having solved for $\mathbf{p}$ in (25), $\mathbf{u}_2$ can be obtained from the first of (24), and then $\mathbf{u} = \tilde{\mathbf{g}} + \mathbf{C}_2^{\mathrm{T}}\mathbf{u}_2$.

2.6. Conjugate gradient algorithm in the pressure formulation

Following Reference [17], the system of equations (25) is solved by a conjugate gradient method. As is well-known, the convergence speed of this iterative method depends highly on the condition of the system matrix $\mathbf{H}_\alpha$. For $\alpha \gg \mu$ in all of Ω, this matrix is well-conditioned and we experience good convergence. However, for α taking values in the region of interest, and more importantly if α is oscillating, the convergence is poor and we conclude that the system needs preconditioning. To this end, a difficulty is that the system matrix is never formed explicitly and hence applying an algebraic preconditioner, such as an incomplete Cholesky factorization or an SSOR preconditioner, would be a cumbersome task. A preconditioning technique based on properties of the underlying partial differential equation was introduced by Cahouet and Chabard [11] and later slightly generalized by Glowinski [12]. As formulated in these two references, the technique is only applicable when α is a positive constant and we therefore use the formulation presented in the following.

To start with, we note that the matrices $\mathbf{B}$, $\mathbf{B}^{\mathrm{T}}$ and $\mathbf{K}_\alpha$ are (formally) discretizations of the operators

$$B = \mathrm{div}$$
$$B^{\mathrm{T}} = -\nabla$$
$$K_\alpha = \alpha I - \mu\Delta$$

and thus the system matrix $\mathbf{H}_\alpha$ may be seen as the discretization of the composed operator

$$H_\alpha = -\mathrm{div}(\alpha I - \mu\Delta)^{-1}\nabla$$

The preconditioning operator is here denoted M_α and is defined by

$$M_\alpha^{-1} q = \varphi_q + \mu q \tag{26}$$

where φ_q is the solution to the boundary value problem

$$\begin{aligned} -\mathrm{div}\left(\frac{1}{\alpha}\nabla\varphi_q\right) &= q \quad \text{in } \Omega \\ \frac{\partial\varphi_q}{\partial n} &= 0 \quad \text{on } \partial\Omega \\ \int_\Omega \varphi_q &= 0 \end{aligned} \tag{27}$$

With this choice, assuming α constant and that the involved differential operators commute, we have

$$\begin{aligned} H_\alpha M_\alpha^{-1} q &= -\mathrm{div}(\alpha I - \mu\Delta)^{-1}\nabla(\varphi_q + \mu q) \\ &= -\mathrm{div}(\alpha I - \mu\Delta)^{-1}\nabla\left(I - \mu\,\mathrm{div}\left(\frac{1}{\alpha}\nabla\right)\right)\varphi_q \\ &= -\mathrm{div}(\alpha I - \mu\Delta)^{-1}\left(I - \mu\,\mathrm{div}\left(\frac{1}{\alpha}\nabla\right)\right)\nabla\varphi_q \\ &= -\mathrm{div}(\alpha I - \mu\Delta)^{-1}(\alpha I - \mu\Delta)\left(\frac{1}{\alpha}\nabla\varphi_q\right) \\ &= -\mathrm{div}\left(\frac{1}{\alpha}\nabla\varphi_q\right) = q \end{aligned}$$

i.e. a perfect preconditioner. Although these calculations require constant α and periodic boundary conditions, see Reference [11], we have experienced a significant improvement when applying this preconditioning strategy. For data used in the numerical examples, typically the number of iterations required for the algorithm to converge is kept below 20.

With $\mathbf{M}_\alpha$ denoting the discretized preconditioning operator, the overall solution algorithm can be described as follows. Let $\mathbf{p}^0$ be arbitrary and calculate $\mathbf{r}^0 = \mathbf{H}_\alpha\mathbf{p}^0 - \mathbf{h}_\alpha$, $\mathbf{z}^0 = \mathbf{M}_\alpha^{-1}\mathbf{r}^0$ and

set $\mathbf{d}^0 = -\mathbf{z}^0$. Then for $k = 0, 1, \ldots$ compute

$$\begin{aligned}
\tau_k &= \mathbf{r}^{k^{\mathrm{T}}}\mathbf{z}^k / \mathbf{d}^{k^{\mathrm{T}}}\mathbf{H}_\alpha \mathbf{d}^k \\
\mathbf{p}^{k+1} &= \mathbf{p}^k + \tau_k \mathbf{d}^k \\
\mathbf{r}^{k+1} &= \mathbf{r}^k + \tau_k \mathbf{H}_\alpha \mathbf{d}^k \\
\mathbf{z}^{k+1} &= \mathbf{M}_\alpha^{-1}\mathbf{r}^{k+1} \\
\beta_k &= \mathbf{r}^{k+1^{\mathrm{T}}}\mathbf{z}^{k+1} / \mathbf{r}^{k^{\mathrm{T}}}\mathbf{z}^k \\
\mathbf{d}^{k+1} &= -\mathbf{z}^{k+1} + \beta_k \mathbf{d}^k
\end{aligned}$$

The algorithm is terminated when $\sqrt{\mathbf{z}^{\mathrm{T}}\mathbf{z}} < 10^{-5}\sqrt{\mathbf{h}_\alpha^{\mathrm{T}}\mathbf{M}_\alpha^{-\mathrm{T}}\mathbf{M}_\alpha^{-1}\mathbf{h}_\alpha}$.

We end this section with some comments regarding a practical implementation of this algorithm. The matrix vector multiplication $\tilde{\mathbf{d}}^k = \mathbf{H}_\alpha \mathbf{d}^k$ is performed in the following five steps: (i) $\tilde{\mathbf{s}}^k = \mathbf{B}^{\mathrm{T}}\mathbf{d}^k$, (ii) $\mathbf{s}^k = \mathbf{C}_2\tilde{\mathbf{s}}^k$, (iii) solve $\mathbf{K}_\alpha \mathbf{t}^k = \mathbf{s}^k$, (iv) $\tilde{\mathbf{t}}^k = \mathbf{C}_2^{\mathrm{T}}\mathbf{t}^k$ and finally (v) $\tilde{\mathbf{d}}^k = \mathbf{B}\tilde{\mathbf{t}}^k$. Steps (ii) and (iv) are virtually a problem of cancelling the degrees of freedom corresponding to the boundary of Ω and are hence easily dealt with. Moreover, the matrix $\mathbf{B}$ is not globally assembled but is stored as a single constant P-element matrix valid for all P-elements (since they are all identical). The steps (i) and (v) consist then of transversing all P-elements and performing matrix vector multiplications on the P-element level and assembling the results. We note that in step (iii), there is no coupling between the x and y degrees of freedom so instead we solve the following two smaller systems of equations

$$\begin{aligned}
\bar{\mathbf{K}}_\alpha \mathbf{t}_x^k &= \mathbf{s}_x^k \\
\bar{\mathbf{K}}_\alpha \mathbf{t}_y^k &= \mathbf{s}_y^k
\end{aligned} \tag{28}$$

The matrix $\bar{\mathbf{K}}_\alpha$ is stored in a banded storage format and is $\mathbf{LDL}^{\mathrm{T}}$-factorized only once in the beginning the algorithm. The solutions $\mathbf{t}_x^k$ and $\mathbf{t}_y^k$ are then obtained by forward and backward substitution, operations that are much cheaper than the factorization of the matrix. Since the size of $\bar{\mathbf{K}}_\alpha$ is only half the size of $\mathbf{K}_\alpha$ and since the factorization is performed only once, this part of the algorithm is efficient both concerning memory storage and computations. For the preconditioning, two systems of equations need to be solved. These systems correspond to the two terms in the definition of the preconditioning operator (26), one used for solving the Poisson-like problem (27) and the other for solving an identity problem. Since these problems are discretized on the mesh of P-elements, they are cheap to solve compared to solving the systems (28) which are discretized on the mesh of U-elements.

3. THE DESIGN OPTIMIZATION PROBLEM

We now consider ρ to be a design variable, or a control function, which affects the (inverted) permeability α, and we write this $\alpha(\rho)$. An example of such a relation is the second of (13), where the control function ρ may be physically interpreted as the distance between two

surfaces encapsulating fluid. However, if the model was to be generalized to three dimensions, the only physically reasonable values of α would be $\alpha = 0$, which corresponds to fluid present, and $\alpha = \infty$, which corresponds to no fluid present. In order to allow for this we therefore consider the situation where α is a fairly general *interpolation function*. We would like ρ to measure the relative amount of fluid at each point in Ω, and the idea is to indicate either nonpresence of fluid by $\rho = 0$ or presence of fluid when $\rho = 1$. Hence, the attempt is that the functions ρ should be approximate characteristic functions of subsets Ω_f of Ω occupied by a fluid. In practice we cannot allow for $\alpha = 0$ or ∞ so we say that $\rho = 0$ should correspond to $\alpha = \bar{\alpha} \gg \mu$ and $\rho = 1$ should correspond to $\alpha = \underline{\alpha} \ll \mu$. The optimization problem, to be stated more precisely later, is to minimize a power function ϕ over all subsets Ω_f with measure $|\Omega_f|$ less than or equal to some specified value, i.e. minimize ϕ with a constraint on available fluid volume.

3.1. The objective function

The chosen objective function to minimize in the design problem is going to be the value of the total potential power evaluated at the solution $\boldsymbol{u}$ to (12), i.e.

$$\phi(\rho) = \min_{\boldsymbol{v} \in \boldsymbol{U}_{\text{div}}} \mathscr{J}_{\alpha(\rho)}(\boldsymbol{v}) = \mathscr{J}_{\alpha(\rho)}(\boldsymbol{u}(\rho)) \tag{29}$$

where $\boldsymbol{u}(\rho)$ is the solution to (12) for $\alpha = \alpha(\rho)$. From the definition of $\mathscr{J}_\alpha(\boldsymbol{u})$ one can immediately conclude that this objective means to minimize the dissipated power $\frac{1}{2}a_\alpha(\boldsymbol{u}, \boldsymbol{u})$ in the fluid plus maximizing the flow velocities at the applied forces $\boldsymbol{f}$.

For an alternative interpretation of the meaning of $\phi(\rho)$ we form another Lagrangian in the minimization of $\boldsymbol{v} \mapsto \mathscr{J}_\alpha(\boldsymbol{v})$ where now the other constraint $\boldsymbol{v} = \boldsymbol{g}$ on $\partial\Omega$ is relaxed,

$$\mathscr{L}_\alpha(\boldsymbol{v}, \boldsymbol{\Lambda}) = \mathscr{J}_\alpha(\boldsymbol{v}) - \langle \boldsymbol{\Lambda}, \boldsymbol{v} - \boldsymbol{g} \rangle_{\partial\Omega}$$

Here we have written $\langle \cdot, \cdot \rangle_{\partial\Omega}$ for the duality pairing between $\boldsymbol{H}^{-1/2}(\partial\Omega)$ and $\boldsymbol{H}^{1/2}(\partial\Omega)$. Let $\boldsymbol{W}_{\text{div}} = \{\boldsymbol{v} \in \boldsymbol{H}^1(\Omega) \,|\, \operatorname{div} \boldsymbol{v} = 0\}$ and look for a saddle point $(\boldsymbol{u}, \lambda) \in \boldsymbol{W}_{\text{div}} \times \boldsymbol{H}^{-1/2}(\partial\Omega)$ one obtains $\boldsymbol{u} = \boldsymbol{g}$ on $\partial\Omega$ and

$$a_\alpha(\boldsymbol{u}, \boldsymbol{v}) - \langle \boldsymbol{f}, \boldsymbol{v} \rangle - \langle \lambda, \boldsymbol{v} \rangle_{\partial\Omega} = 0 \quad \forall \boldsymbol{v} \in \boldsymbol{W}_{\text{div}} \tag{30}$$

Choosing $\boldsymbol{v} = \boldsymbol{u}$ in (30) and plugging the resulting expression into (14) one obtains

$$\mathscr{J}_\alpha(\boldsymbol{u}) = \tfrac{1}{2}(\langle \lambda, \boldsymbol{g} \rangle_{\partial\Omega} - \langle \boldsymbol{f}, \boldsymbol{u} \rangle)$$

or when writing it as a function of ρ,

$$\phi(\rho) = \mathscr{J}_{\alpha(\rho)}(\boldsymbol{u}(\rho)) = \tfrac{1}{2}(\langle \lambda(\rho), \boldsymbol{g} \rangle_{\partial\Omega} - \langle \boldsymbol{f}, \boldsymbol{u}(\rho) \rangle) \tag{31}$$

Hence the design goal is to minimize $\langle \lambda(\rho), \boldsymbol{g} \rangle_{\partial\Omega} - \langle \boldsymbol{f}, \boldsymbol{u}(\rho) \rangle$, which can be described as a combination of minimizing the forces on the boundary λ required to propel the fluid to obtain the fixed velocities $\boldsymbol{g}$ on the boundary, and maximizing flow velocities $\boldsymbol{u}$ at the areas where fixed forces $\boldsymbol{f}$ are applied.

Consider the common special case $\boldsymbol{f} = \boldsymbol{0}$. Then, again from the original definition of $\mathscr{J}_\alpha(\boldsymbol{u})$, one sees that this objective means to minimize the dissipated power in the fluid. This can also be described as minimizing the average pressure drop under the additional assumption $\bar{\boldsymbol{g}} = \bar{g}\boldsymbol{n}$, see the appendix.

3.2. Statement of the optimization problem

Let the set of admissible controls be

$$\mathscr{H} = \left\{ \rho \in L^\infty(\Omega) \,\middle|\, 0 \leqslant \rho \leqslant 1 \text{ a.e. in } \Omega, \quad \int_\Omega \rho \leqslant \gamma |\Omega| \right\}$$

with γ being the prescribed volume fraction, a constant between 0 and 1. Furthermore, let $\alpha : [0,1] \to [\underline{\alpha}, \bar{\alpha}]$ be a decreasing, convex and continuously differentiable interpolation function. We consider the following three optimization problems:

$$\begin{aligned} &\min_{(\rho,\boldsymbol{u}) \in \mathscr{H} \times \boldsymbol{U}_{\text{div}}} \quad \mathscr{J}_{\alpha(\rho)}(\boldsymbol{u}) \\ &\min_{\rho \in \mathscr{H}} \quad \phi(\rho) \\ &\min_{\boldsymbol{u} \in \boldsymbol{U}_{\text{div}}} \quad \psi(\boldsymbol{u}) \end{aligned} \tag{32}$$

where ψ is defined by

$$\psi(\boldsymbol{u}) = \min_{\rho \in \mathscr{H}} \quad \mathscr{J}_{\alpha(\rho)}(\boldsymbol{u}) \tag{33}$$

It can be shown that these three problems are equivalent in the sense that if a pair $(\rho^*, \boldsymbol{u}^*)$ is a solution to any one of the problems,[‡] it is also a solution to the other two. It follows that if one of the problems is well-posed, i.e. the set of solutions is nonempty, then the other two are also well-posed. Regarding the question of existence of solutions, we may therefore restrict ourselves to examining only one of the three problems.

Theorem 3.1

The first of (32) is well-posed.

Proof

Let $\{(\rho_n, \boldsymbol{u}_n)\}_{n=1}^\infty \subset \mathscr{H} \times \boldsymbol{U}_{\text{div}}$ be a minimizing sequence of $\mathscr{J}_\alpha$. Since $\mathscr{H}$ is weakly* compact, there is an element $\rho^* \in \mathscr{H}$ and a subsequence, denoted $\{\rho_m\}_{m=1}^\infty$, so that $\rho_m \to \rho^*$ weakly* in $L^\infty(\Omega)$. Furthermore, since α is positive and bounded from above and below, the bilinear form a_α in (14) is $\boldsymbol{H}^1(\Omega)$-elliptic, and it follows that $\{\boldsymbol{u}_n\}_{n=1}^\infty \subset \boldsymbol{H}^1(\Omega)$ is relatively weakly compact. Since $\boldsymbol{U}_{\text{div}} \subset \boldsymbol{H}^1(\Omega)$ is weakly closed, there is an element $\boldsymbol{u}^* \in \boldsymbol{U}_{\text{div}}$ so that, again for a subsequence $\{\boldsymbol{u}_m\}_{m=1}^\infty$, $\boldsymbol{u}_m \to \boldsymbol{u}^*$ weakly in $\boldsymbol{H}^1(\Omega)$. Naturally these two subsequences can be chosen as a subsequence of the originally minimizing sequence and, in addition, they can be chosen so that $\boldsymbol{u}_m \to \boldsymbol{u}^*$ strongly in $\boldsymbol{L}^2(\Omega)$ because of the compact inclusion $\boldsymbol{H}^1(\Omega) \subset \boldsymbol{L}^2(\Omega)$. We now show that $\mathscr{J}_\alpha$ is lower semicontinuous with respect to this topology.

We only show lower semicontinuity of the term that depends on α, treatment of the other terms are classical and can be found in e.g. [18]. We have

$$\begin{aligned} &\int_\Omega \alpha(\rho_m) \boldsymbol{u}_m \cdot \boldsymbol{u}_m - \int_\Omega \alpha(\rho^*) \boldsymbol{u}^* \cdot \boldsymbol{u}^* \\ &\quad = \int_\Omega \alpha(\rho_m)(\boldsymbol{u}_m \cdot \boldsymbol{u}_m - \boldsymbol{u}^* \cdot \boldsymbol{u}^*) + \int_\Omega (\alpha(\rho_m) - \alpha(\rho^*)) \boldsymbol{u}^* \cdot \boldsymbol{u}^* \end{aligned}$$

[‡]To avoid confusion, $(\rho^*, \boldsymbol{u}^*)$ is termed a solution to the second of (32) if (i) $\boldsymbol{u}^* = \boldsymbol{u}(\rho^*)$ in (29) and if (ii) ρ^* solution to the second of (32). An analogous definition is assumed for the third of (32).

where the two terms on the right hand side can be treated individually as follows. The first term tends to zero since

$$\left|\int_\Omega \alpha(\rho_m)(\boldsymbol{u}_m\cdot\boldsymbol{u}_m-\boldsymbol{u}^*\cdot\boldsymbol{u}^*)\right| \leqslant \int_\Omega |\alpha(\rho_m)(\boldsymbol{u}_m\cdot\boldsymbol{u}_m-\boldsymbol{u}^*\cdot\boldsymbol{u}^*)|$$
$$\leqslant C_1\int_\Omega |\boldsymbol{u}_m\cdot\boldsymbol{u}_m-\boldsymbol{u}^*\cdot\boldsymbol{u}^*| = C_1\int_\Omega |(\boldsymbol{u}_m-\boldsymbol{u}^*)\cdot(\boldsymbol{u}_m+\boldsymbol{u}^*)|$$
$$\leqslant C_1\|\boldsymbol{u}_m-\boldsymbol{u}^*\|_0\|\boldsymbol{u}_m+\boldsymbol{u}^*\|_0 \leqslant C_2\|\boldsymbol{u}_m-\boldsymbol{u}^*\|_0$$

and $\boldsymbol{u}_m\to\boldsymbol{u}^*$ in $\boldsymbol{L}^2(\Omega)$. Since $\boldsymbol{u}^*\cdot\boldsymbol{u}^*\geqslant 0$ pointwise, the second term can be estimated as follows

$$\int_\Omega(\alpha(\rho_m)-\alpha(\rho^*))\boldsymbol{u}^*\cdot\boldsymbol{u}^* \geqslant \int_\Omega(\rho_m-\rho^*)\alpha'(\rho^*)\boldsymbol{u}^*\cdot\boldsymbol{u}^*$$

where we have used that α is convex and continuously differentiable. Since α' is bounded from above and below, $\alpha'(\rho^*)\boldsymbol{u}^*\cdot\boldsymbol{u}^*\in L^1(\Omega)$ and the right hand side tends to zero because of weak* convergence of ρ_m to ρ^*. This shows that $\mathscr{J}_\alpha$ is lower semicontinuous.

It now follows that for any $(\rho,\boldsymbol{u})\in\mathscr{H}\times\boldsymbol{U}_{\mathrm{div}}$

$$\mathscr{J}_{\alpha(\rho^*)}(\boldsymbol{u}^*)\leqslant\liminf_{m\to\infty}\ \mathscr{J}_{\alpha(\rho_m)}(\boldsymbol{u}_m)\leqslant\mathscr{J}_{\alpha(\rho)}(\boldsymbol{u})$$

i.e. $(\rho^*,\boldsymbol{u}^*)\in\mathscr{H}\times\boldsymbol{U}_{\mathrm{div}}$ solves the first of (32). □

The second and third of (32) are nested formulations of the first, which is formulated as a simultaneous analysis and design problem. The second of (32) is the problem for which the objective function is examined in detail in Section 3.1 and that is solved in practice. Now consider the special case of linear interpolation, i.e. $\alpha(\rho)=\bar{\alpha}+(\underline{\alpha}-\bar{\alpha})\rho$, and, for any $\boldsymbol{u}\in\boldsymbol{U}_{\mathrm{div}}$, let $\Omega(\boldsymbol{u})\subset\Omega$ be a set with $|\Omega(\boldsymbol{u})|=\gamma|\Omega|$ that fulfils

$$\boldsymbol{x}\in\Omega(\boldsymbol{u})\Rightarrow\boldsymbol{u}(\boldsymbol{x})\cdot\boldsymbol{u}(\boldsymbol{x})\geqslant\boldsymbol{u}(\boldsymbol{y})\cdot\boldsymbol{u}(\boldsymbol{y}),\quad\forall\boldsymbol{y}\in\Omega\backslash\Omega(\boldsymbol{u})$$

It is easy to see that such a set exists and that a solution to the inner minimization problem in the definition of ψ (33) is given by $\rho(\boldsymbol{u})=\chi_{\Omega(\boldsymbol{u})}$, i.e. the characteristic function of the set $\Omega(\boldsymbol{u})$. In other words, when the interpolation is linear we can always find an optimal design function ρ^* in the set

$$\tilde{\mathscr{H}}=\left\{\rho\in L^\infty(\Omega)\,\middle|\,\rho(\boldsymbol{x})\in\{0,1\}\ \text{a.e. in }\Omega,\quad\int_\Omega\rho\leqslant\gamma|\Omega|\right\}$$

Since $\tilde{\mathscr{H}}\subset\mathscr{H}$, we have proved the following

Corollary 3.1
The first of (32) is well-posed with $\mathscr{H}$ substituted for $\tilde{\mathscr{H}}$.

Theorem 3.1 and Corollary 3.1 state indirectly that there is no need for a regularization of the optimization problem, even if ρ is only allowed to take values 0 or 1. This is a rather unusual situation in topology optimization of continua and is physically a consequence of how power is dissipated in Stokes flow, something that is commented upon throughout Section 4.

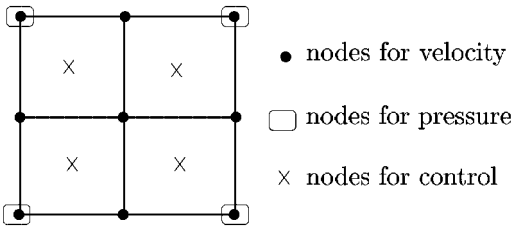

Figure 2. Quadrilateral finite elements used for the continuous bilinear approximation of velocity and pressure and piecewise constant approximation of control.

3.3. *Finite element discretization of the optimization problem*

We have supposed that Ω is partitioned into $m = 4N_x \times N_y$ mutually disjoint U-elements Ω_i, such that $\Omega_i \subset \Omega$ and $\bigcup_{i=1}^{m} \bar{\Omega}_i = \bar{\Omega}$. For each partition, h denotes a characteristic size of the (largest) element and L_h the space of U-elementwise constant functions on Ω. We approximate the *control function* ρ as *U-elementwise constant*, which means that the discretized controls will be restricted to belong to the set $\mathscr{H}_h = \mathscr{H} \cap L_h$. The picture in Figure 2 shows the resulting quadrilateral finite elements used for the approximation of velocity, pressure and control.

The operator $\mathscr{P}_h$ is defined as the U-elementwise constant interpolation

$$\mathscr{P}_h \rho = \sum_{i=1}^{m} \rho_i \chi_{\Omega_i}$$

where ρ_i is the integral mean of ρ over Ω_i, i.e.

$$\rho_i = \frac{1}{|\Omega_i|} \int_{\Omega_i} \rho$$

It can be verified that $\mathscr{P}_h$ maps $\mathscr{H}$ onto $\mathscr{H}_h$ and that $\mathscr{P}_h \rho$ converges to ρ in $L^2(\Omega)$-norm for any $\rho \in \mathscr{H}$.[§]

We pose two very weak assumptions on the discretization of the state problem. Standard interpolation estimates, see Reference [19], together with the density of smooth functions give that we can assume that the discretized functions are *dense* in the exact ones:

$$\text{(I)} \quad \forall (\boldsymbol{u}, p) \in \boldsymbol{U} \times \Pi\text{: } \lim_{h \to 0} \inf_{\boldsymbol{v}_h \in \boldsymbol{U}_h} \|\boldsymbol{u} - \boldsymbol{v}_h\|_1 = \lim_{h \to 0} \inf_{q_h \in \Pi_h} \|p - q_h\|_0 = 0$$

Moreover, we pose the following *closedness* property:

$$\text{(II)} \quad \boldsymbol{u}_h \in \boldsymbol{U}_h, \quad \boldsymbol{u}_h \to \boldsymbol{u} \text{ weakly in } \boldsymbol{H}^1(\Omega) \Rightarrow \boldsymbol{u} \in \boldsymbol{U}$$

which follows immediately if e.g. $\boldsymbol{U}_h \subset \boldsymbol{U}$.

The *FE-discretized optimization problem* can, in one of its equivalent forms, be stated as

$$\min_{(\rho_h, \boldsymbol{u}_h) \in \mathscr{H}_h \times \boldsymbol{U}_{\text{div},h}} \quad \mathscr{J}_{\alpha(\rho_h)}(\boldsymbol{u}_h) \tag{34}$$

[§]The convergence refers to the sequence obtained when letting $h \to 0$ from above, which is often implicitly understood in this text.

in which $\boldsymbol{U}_{\mathrm{div},h}$ is the set of functions in $\boldsymbol{U}_h$ for which the discretized incompressibility condition, second of (15), holds.

We have the following *density and closedness lemmas* for the discretization of $\boldsymbol{U}_{\mathrm{div}}$:

Lemma 3.1
Suppose that (I) and the LBB-condition (17) hold true, and let $\boldsymbol{u}$ be any function in $\boldsymbol{U}_{\mathrm{div}}$. Then there exist functions $\boldsymbol{u}_h \in \boldsymbol{U}_{\mathrm{div},h}$ such that $\boldsymbol{u}_h \to \boldsymbol{u}$ strongly in $\boldsymbol{H}^1(\Omega)$.

Proof
Let $\boldsymbol{u}$ be any function in $\boldsymbol{U}_{\mathrm{div}}$. Project $\boldsymbol{u}$ onto the set $\boldsymbol{U}_{\mathrm{div},h}$ to obtain $\boldsymbol{u}_h$. If the projection is performed in the sense of the power norm $\sqrt{a_\alpha(\cdot,\cdot)}$ for any fixed α, then $\boldsymbol{u}_h$ is governed by (15) with $\langle \boldsymbol{f}, \cdot \rangle = a_\alpha(\boldsymbol{u}, \cdot)$. Similarly we can project $\boldsymbol{u}$ on $\boldsymbol{U}_{\mathrm{div}}$ to get $\boldsymbol{u}$ itself, so $\boldsymbol{u}$ is governed by (12) with $\langle \boldsymbol{f}, \cdot \rangle = a_\alpha(\boldsymbol{u}, \cdot)$. Hence, having assumed (17), the error estimate (18) applies. Therefore $\|\boldsymbol{u}_h - \boldsymbol{u}\|_1$ converges to zero since we have also assumed (I). □

Lemma 3.2
Suppose that (I) and (II) hold true, and let $\boldsymbol{u}_h \in \boldsymbol{U}_{\mathrm{div},h}$ be functions such that $\boldsymbol{u}_h \to \boldsymbol{u}$ weakly in $\boldsymbol{H}^1(\Omega)$. Then $\boldsymbol{u}$ belongs to $\boldsymbol{U}_{\mathrm{div}}$.

Proof
By (II), $\boldsymbol{u} \in \boldsymbol{U}$, so it remains to show only $b(\boldsymbol{u}, q) = 0$ in which q is an arbitrary choice from Π.

By (I) one can find $q_h \in \Pi_h$ such that $q_h \to q$ strongly in $L^2(\Omega)$. This together with the weak convergence of $\boldsymbol{u}_h$ ensure

$$b(\boldsymbol{u}, q) = \lim_{h \to 0} b(\boldsymbol{u}_h, q) + \lim_{h \to 0} b(\boldsymbol{u}_h, q_h - q) = \lim_{h \to 0} b(\boldsymbol{u}_h, q_h)$$

It holds that $b(\boldsymbol{u}_h, q_h) = 0$ since $\boldsymbol{u}_h \in \boldsymbol{U}_{\mathrm{div},h}$, and therefore $b(\boldsymbol{u}, q) = 0$. □

Now we are in a position to prove *convergence of the finite element scheme*:

Theorem 3.2
Suppose that (I), (II) and the LBB-condition (17) hold true, and let $\{(\rho_h^*, \boldsymbol{u}_h^*)\}$ be a sequence of solutions to (34) as $h \to 0$. Then there exists an element $(\rho^*, \boldsymbol{u}^*)$ which is feasible in the first of (32), and there is a subsequence, again denoted by $\{(\rho_h^*, \boldsymbol{u}_h^*)\}$, such that

$$\rho_h^* \to \rho^* \quad \text{weakly}^* \text{ in } L^\infty(\Omega)$$

$$\boldsymbol{u}_h^* \to \boldsymbol{u}^* \quad \text{weakly in } \boldsymbol{H}^1(\Omega)$$

Moreover, any such limit $(\rho^*, \boldsymbol{u}^*)$ solves the first of (32).

Proof
Since the functional $\mathscr{J}_{\alpha(\rho_h^*)}(\cdot)$ is uniformly elliptic and the sets $\mathscr{H}_h$ are uniformly bounded with respect to h, it follows that the sequence $\{\boldsymbol{u}_h^*\}$ is bounded in $\boldsymbol{H}^1(\Omega)$ and $\{\rho_h^*\}$ is bounded in $L^\infty(\Omega)$. Hence we can extract a subsequence, again denoted $\{(\rho_h^*, \boldsymbol{u}_h^*)\}$, such that ρ_h^* converges weakly* in $L^\infty(\Omega)$ to a limit ρ^* and $\boldsymbol{u}_h^*$ converges weakly in $\boldsymbol{H}^1(\Omega)$ (and strongly in $\boldsymbol{L}^2(\Omega)$) to a limit $\boldsymbol{u}^*$. By Lemma 3.2, $\boldsymbol{u}^* \in \boldsymbol{U}_{\mathrm{div}}$, and since $\mathscr{H}_h \subset \mathscr{H}$ where $\mathscr{H}$ is weakly* closed, $\rho^* \in \mathscr{H}$, and therefore $(\rho^*, \boldsymbol{u}^*)$ is feasible in the first of (32).

Pick any feasible pair $(\rho, \boldsymbol{u})$ in the first of (32). By Lemma 3.1 there exists $\boldsymbol{u}_h \in \boldsymbol{U}_{\mathrm{div},h}$ such that $\boldsymbol{u}_h$ converges to $\boldsymbol{u}$ strongly in $\boldsymbol{H}^1(\Omega)$. Moreover, $(\mathscr{P}_h\rho, \boldsymbol{u}_h)$ is feasible in (34), so

$$\mathscr{J}_{\alpha(\rho_h^*)}(\boldsymbol{u}_h^*) \leqslant \mathscr{J}_{\alpha(\mathscr{P}_h\rho)}(\boldsymbol{u}_h) \tag{35}$$

By the arguments on lower semicontinuity in Theorem 3.1, $\liminf \mathscr{J}_{\alpha(\rho_h^*)}(\boldsymbol{u}_h^*)$ is bounded below by $\mathscr{J}_{\alpha(\rho^*)}(\boldsymbol{u}^*)$, and $\mathscr{J}_{\alpha(\mathscr{P}_h\rho)}(\boldsymbol{u}_h)$ converges to $\mathscr{J}_{\alpha(\rho)}(\boldsymbol{u})$ by the strong convergence of $\mathscr{P}_h\rho$ in $L^2(\Omega)$ and $\boldsymbol{u}_h$ in $\boldsymbol{H}^1(\Omega)$, cf. Reference [20]. Therefore, taking the limit of (35) results in

$$\mathscr{J}_{\alpha(\rho^*)}(\boldsymbol{u}^*) \leqslant \lim_{h\to 0} \inf \mathscr{J}_{\alpha(\rho_h^*)}(\boldsymbol{u}_h^*) \leqslant \lim_{h\to 0} \mathscr{J}_{\alpha(\mathscr{P}_h\rho)}(\boldsymbol{u}_h) = \mathscr{J}_{\alpha(\rho)}(\boldsymbol{u})$$

which means that $(\rho^*, \boldsymbol{u}^*)$ is optimal in the first of (32). □

The result establishes the convergence of optimal control functions ρ_h^*, obtained by solving the finite element discretized optimization problem, to optimal control functions ρ^* in the original problem statement. The convergence is only in a weak* sense, so this fact alone does not rule out the existence of checkerboard patterns in the fields ρ_h^*. If such patterns appear, however, it is clear how to interpret them, namely as a convergence to intermediate 'gray' control values. As the choice of $\rho \mapsto \alpha(\rho)$ is such that the final controls will be almost completely 'black-white', however, checkerboards will not appear. In fact, it follows from Corollary 3.2 in [20] that ρ_h^* converges strongly to ρ^* in $L^p(\Omega_b)$-norm, where Ω_b is the subset of Ω where ρ^* equals 0 or 1, and $p \in [1, \infty)$ is arbitrary.

3.4. Sequential separable and convex programming

As a base for a numerical solution procedure, we use the nested problem formulation given by the second of (32). In this section we present the discretized version of this problem and how it is solved.

Let $\boldsymbol{\rho}$ be the vector of U-elementwise constant values of ρ_h, and $\mathbf{u}_2(\boldsymbol{\rho})$ and $\mathbf{p}(\boldsymbol{\rho})$ the vectors that solve (24) for this ρ_h. Furthermore, we set $\mathbf{u}(\boldsymbol{\rho}) = \tilde{\mathbf{g}} + \mathbf{C}_2^{\mathrm{T}}\mathbf{u}_2(\boldsymbol{\rho})$ and emphasise that $\tilde{\mathbf{K}}_\alpha$ depends on $\boldsymbol{\rho}$ by denoting it $\tilde{\mathbf{K}}(\boldsymbol{\rho})$, i.e.

$$\tilde{\mathbf{K}}(\boldsymbol{\rho}) = \sum_{i=1}^{m} (\alpha(\rho_i)\mathbf{K}_i^{\alpha} + \mu\mathbf{K}_i^{\mu}) \tag{36}$$

where $\mathbf{K}_i^{\alpha}$ and $\mathbf{K}_i^{\mu}$ are element matrices arising from the terms in the first of (13). The discrete version of the objective function ϕ given by (29) can now be written as

$$\Phi(\boldsymbol{\rho}) = \tfrac{1}{2}(\mathbf{u}(\boldsymbol{\rho})^{\mathrm{T}}(\tilde{\mathbf{K}}(\boldsymbol{\rho})\tilde{\mathbf{g}} - \mathbf{C}_2^{\mathrm{T}}\mathbf{F}) + \mathbf{p}(\boldsymbol{\rho})^{\mathrm{T}}\mathbf{B}\tilde{\mathbf{g}}) \tag{37}$$

This expression can be verified by expanding the individual terms in the right hand side of (37), using the expression for $\mathbf{u}(\boldsymbol{\rho})$ above and Equation (24), and comparing this expansion with the right hand side of (22) with $\mathbf{v}_2 = \mathbf{u}_2(\boldsymbol{\rho})$. The reason for not using (22) with $\mathbf{v}_2 = \mathbf{u}_2(\boldsymbol{\rho})$ as an expression for the objective function is that (37) is more convenient when considering an implementation. The vectors $\tilde{\mathbf{K}}(\boldsymbol{\rho})\tilde{\mathbf{g}} - \mathbf{C}_2^{\mathrm{T}}\mathbf{F}$ and $\mathbf{B}\tilde{\mathbf{g}}$ are (virtually) the right hand sides of (24) and are needed for obtaining $\mathbf{u}(\boldsymbol{\rho})$ and $\mathbf{p}(\boldsymbol{\rho})$ in the first place. The objective value is then simply obtained by performing two scalar products followed by an addition and a multiplication.

From a mathematical programming point of view, the discrete version of the second of (32) is conveniently written as

$$\begin{cases} \min\limits_{\boldsymbol{\rho}} & \Phi(\boldsymbol{\rho}) \\ \text{s.t.} & \mathbf{e}^{\mathrm{T}}\boldsymbol{\rho} \leqslant \gamma|\Omega| \\ & \mathbf{0} \leqslant \boldsymbol{\rho} \leqslant \mathbf{1} \end{cases}$$

in which $\mathbf{e}$ is the vector containing the U-element areas. This problem is solved by means of sequential separable and convex programming. In iteration k and for a design suggestion $\boldsymbol{\rho}^k$, the vectors $\mathbf{u}(\boldsymbol{\rho}^k)$ and $\mathbf{p}(\boldsymbol{\rho}^k)$ are obtained and the following separable and convex subproblem is formed:

$$\begin{cases} \min\limits_{\boldsymbol{\rho}} & r^k + \sum_{i=1}^{m} \dfrac{q_i^k}{\rho_i - l_i^k} \\ \text{s.t.} & \mathbf{e}^{\mathrm{T}}\boldsymbol{\rho} \leqslant \gamma|\Omega| \\ & \underline{\boldsymbol{\rho}}^k \leqslant \boldsymbol{\rho} \leqslant \bar{\boldsymbol{\rho}}^k \end{cases} \tag{38}$$

where ρ_i are the element values of $\boldsymbol{\rho}$. The expression for the objective function in (38) is known as an MMA-expansion and was introduced by Svanberg [21]. The parameters l_i^k, $\underline{\boldsymbol{\rho}}^k$ and $\bar{\boldsymbol{\rho}}^k$ are parameters that are dynamically updated between iterations according to the scheme in [21]. The parameters r^k and the q_i^k are then chosen so that function values and first order derivatives are correct in the current iteration point $\boldsymbol{\rho}^k$. For this, a sensitivity analysis is required for the objective function. We set $\alpha(\boldsymbol{\rho}) = \alpha(\rho_h)$ and note that the objective function is (20) with $\mathbf{v} = \mathbf{u}(\boldsymbol{\rho})$, i.e.,

$$\Phi(\boldsymbol{\rho}) = J_{\alpha(\boldsymbol{\rho})}(\mathbf{u}(\boldsymbol{\rho})) = \min_{\mathbf{v}} J_{\alpha(\boldsymbol{\rho})}(\mathbf{v}) \tag{39}$$

in which the minimization is performed subject to constraints (21). The function Φ can obviously be written as pointwise maxima of an indexed family of functions, and so we can apply theorems on generalized gradients for such functions. In fact, it follows from Theorem 2.8.6 in Reference [22] that

$$\frac{\partial \Phi(\boldsymbol{\rho})}{\partial \rho_i} = \frac{1}{2}\mathbf{u}(\boldsymbol{\rho})^{\mathrm{T}} \frac{\partial \tilde{\mathbf{K}}(\boldsymbol{\rho})}{\partial \rho_i}\mathbf{u}(\boldsymbol{\rho})$$

since the minimizing vector $\mathbf{u}(\boldsymbol{\rho})$ in (39) is always unique. Using (36) this becomes

$$\frac{\partial \Phi(\boldsymbol{\rho})}{\partial \rho_i} = \frac{1}{2}\alpha'(\rho_i)\mathbf{u}(\boldsymbol{\rho})^{\mathrm{T}}\mathbf{K}_i^{\alpha}\mathbf{u}(\boldsymbol{\rho})$$

Whence $\alpha'(\rho_i) \leqslant 0$ and $\mathbf{u}(\boldsymbol{\rho})^{\mathrm{T}}\mathbf{K}_i^{\alpha}\mathbf{u}(\boldsymbol{\rho}) \geqslant 0$, it follows that one will improve the objective, or at least not worsen it, when one adds fluid to any part of Ω. Note that since all U-elements are identical, only two representatives of the element matrices need to be stored and the calculation of sensitivities as well as assembly of the global stiffness matrix are cheap operations. When (38) is completely determined, it is (due to separability, convexity and only one constraint) solved cheaply using a dual method and the solution is taken as a new design suggestion $\boldsymbol{\rho}^{k+1}$. This iterative procedure is stopped when the relative difference between two successive objective values is less than 10^{-5} twice in a row.

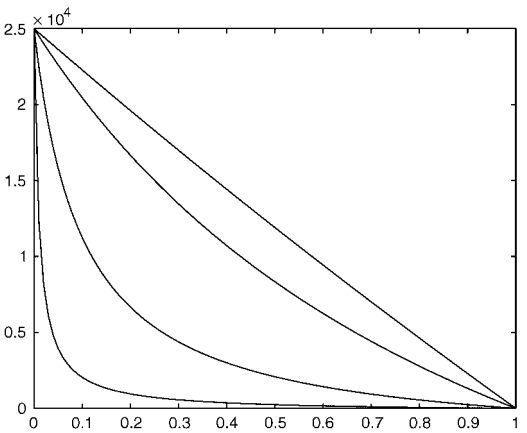

Figure 3. The interpolation function (40) plotted for $q = 0.01$, 0.1, 1 and 10.

4. NUMERICAL EXAMPLES

4.1. Preliminaries

We begin this section by discussing the choice of interpolation function $\rho \mapsto \alpha(\rho)$. Since the goal is for ρ to only take values 0 or 1, the idea is to choose α in such a way that intermediate values of ρ are suppressed. From this point of view, it is interesting to note that the discussion leading to Corollary 3.1 indicates that α should be linear in order to end up with a discrete-valued solution. However, a linear interpolation function would impose a too severe penalty on the design and we would often end up with locally (and non-globally) optimal solutions. Therefore we use the following convex and q-parameterized interpolation function:

$$\alpha_q(\rho) = \bar{\alpha} + (\underline{\alpha} - \bar{\alpha})\rho\frac{1+q}{\rho+q} \tag{40}$$

The parameter $q > 0$ is a penalty parameter that is used to control the level of 'gray' in the optimal design. This function is depicted in Figure 3 for four different values of q and parameter values that are used in all numerical examples, $\mu = 1$, $\underline{\alpha} = 2.5\mu/100^2$ and $\bar{\alpha} = 2.5\mu/0.01^2$. It is easily deduced that when q is large, the interpolation is close to linear which likely would encourage a discrete-valued optimal solution.

The profile of nonzero prescribed flow velocities on the boundary is always (except for in the rugby ball example in Section 4.4) parabolic shaped and the magnitude of the velocity can be written $g = \bar{g}(1 - (2t/l)^2)$, parameterized in $t \in [-l/2, l/2]$. Here l is the length of the boundary part where the flow velocity is prescribed and $\bar{g}$ is the magnitude of the flow velocity at the centre of this boundary part. The direction of the flow and the value of the parameter l will be found from figures and the value of the parameter $\bar{g}$ will be given in the text.

In order to obtain a sufficiently discrete-valued solution, a penalty parameter value of $q = 0.1$ is used. Because of nonconvexity, we have on occasion experienced problems with locally optimal solutions when solving the problems directly using these parameter values. For some

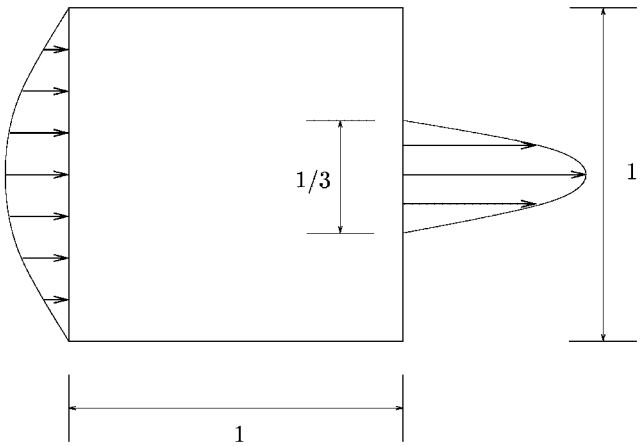

Figure 4. Design domain for the diffuser example. The outlet is centred on the right side of the domain.

of the examples we therefore consider a two-step solution procedure where the problem is initially solved with a small penalty value of $q = 0.01$. The obtained solution is used as an initial guess for the problem with a penalty value of $q = 0.1$. This is done with all other parameters unchanged. The main idea is to generate a clever initial guess for the ill-conditioned (in terms of convexity) optimization problem by initially solving a well-conditioned one. Whether or not this strategy is applied, we have always started from a constant initial guess $\rho = \gamma$, where γ is the prescribed volume fraction, and the iteration numbers given in the tables are the total number of iterations needed to obtain the optimal solution starting from this constant design.

Finally, in the grey scale pictures showing the optimal results, black corresponds to a design value of $\rho = 0$ and white a value of $\rho = 1$.

4.2. A diffuser

The first two examples are engineering applications commonly found in the fluid mechanics literature. Although these examples may be more interesting when considering more complicated fluid models, they are here used to give a first illustration and verification of the methodology presented in this paper. The first example is the diffuser that is depicted in Figure 4. The prescribed volume fraction is $\gamma = 0.5$ and the maximum flow velocity is $\bar{g} = 1$ at the inlet on the left and $\bar{g} = 3$ at the outlet on the right. The problem is solved directly for two mesh discretizations, a coarse and a fine mesh, and the solutions are shown in Figure 5. Apart from illustrating mesh independence, the solutions can be compared with the ones obtained by Çabuk and Modi [6]. In Reference [6], a similar diffuser problem is solved using shape optimization in Navier–Stokes equations for low Reynolds numbers. A major difference from here is that the outflow condition (actually corresponding to the inflow condition on the left side of the domain in Figure 4) is of Neumann type, which, together with some other differences, make the solutions look rather different from a global perspective. However, when comparing the boundary shapes closer to the side where a Dirichlet parabolic flow profile is prescribed, they are similar. We believe that the solutions here would be different if one

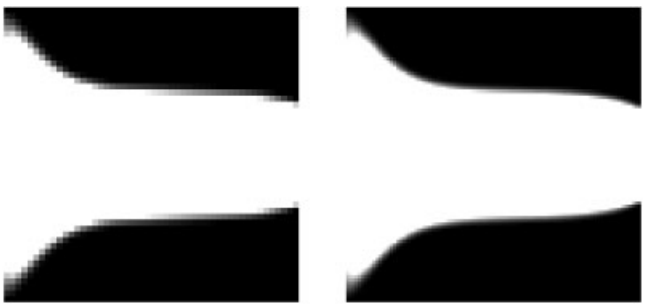

Figure 5. Optimal diffuser on a coarse and a fine finite element mesh.

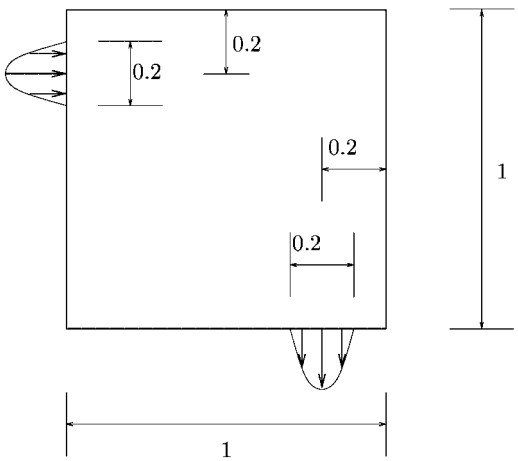

Figure 6. Design domain for the pipe bend example.

includes the possibility of combining the parabolic flow profile conditions on the boundary with for instance constant flow profiles or Neumann boundary conditions.

4.3. *A pipe bend*

We follow up the previous example with a pipe bend shown in Figure 6. Here $\gamma = 0.08\pi$ and $\bar{g} = 1$ for the prescribed inflow and outflow. The prescribed volume fraction is chosen so that the optimal solution has the same volume as a quarter torus of inner radius 0.7 and outer radius 0.9 that exactly fits to the inlet and outlet. The solution strategy and other input data are the same as for the diffuser example and the solutions are shown in Figure 7. As can be seen, the optimal solution is a straight pipe connecting the inlet and outlet and not, as pipe bends in fluid mechanics literature mostly are, torus shaped, which can be explained as follows. If a prescribed amount of fluid is to be transported in a pipe, the shears in the fluid are large when the pipe is thin and, conversely, small when the pipe is wide. Since the dissipated power in Stokes flow is due to shears only, an optimal flow pipe is preferably short and wide. If for instance a flow model that allows for separation of the boundary layer would

Figure 7. Optimal pipe bend on a coarse and a fine finite element mesh.

Table I. Computational data for the diffuser.

Number of U-elements	Number of iterations	Objective value
50×50	29	30.59
100×100	33	30.46

Table II. Computational data for the pipe bend.

Number of U-elements	Number of iterations	Objective value
50×50	64	10.01
100×100	85	9.76

have been used, the solutions in Figure 7 would be rather poor and a more torus shaped solution would probably be more advantageous. Computational data for the diffuser and the pipe bend can be found in Tables I and II, respectively.

4.4. A rugby ball

The design domain for the third numerical example is shown in Figure 8 and is for the computations discretized into 100×100 U-elements. The prescribed velocity on the boundary is constant, directed upwards and of magnitude 1. A small portion of the design domain close to the boundary is prescribed fluid and the remainder of the domain is subject to the optimization. The problem is solved for three values of γ, and the results are shown in Figure 9. It is seen that the optimal shape is insensitive to the prescribed volume fraction γ and reminds of that of a rugby ball. A very similar example has been treated theoretically in the context of shape optimization in Stokes flow by Pironneau [3, 4]. There it is for instance concluded that the wedge at the front and back of the optimal shape is necessarily of angle 90°, which seems to agree reasonably well with the obtained numerical results. From a numerical viewpoint, this problem is well-conditioned and little or no precautionary measures need to be taken. The solution procedure presented in Section 4.1 is used here and data for this example can be found in Table III.

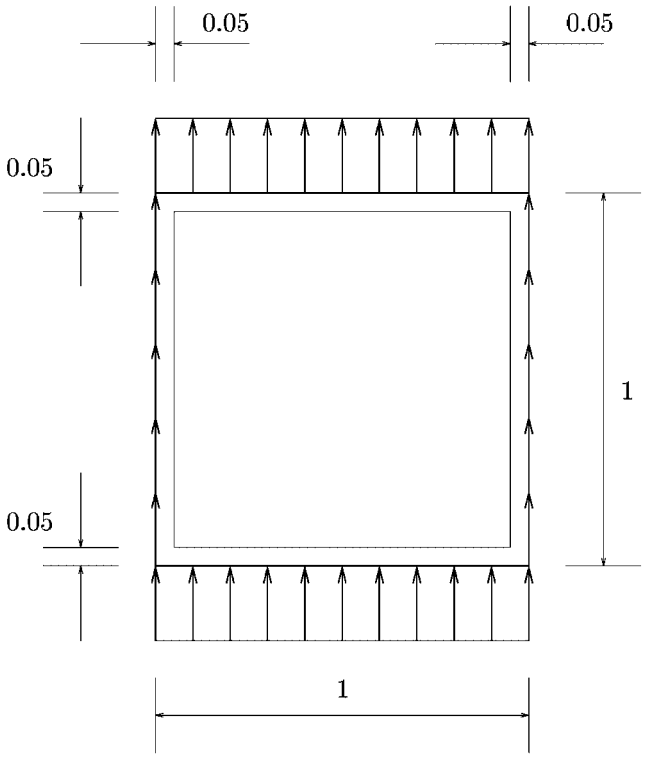

Figure 8. Design domain for the rugby ball example.

Figure 9. Optimal rugby balls for $\gamma = 0.8$, 0.9 and 0.95.

4.5. A double pipe

In Figure 10, a parameterized design domain is shown. The maximum velocities at the inlets and outlets are defined by $\bar{g} = 1$ and the prescribed volume fraction is chosen as $\gamma = \frac{1}{3}$. The

Table III. Computational data for the rugby ball.

Volume fraction γ	Number of iterations	Objective value
0.8	47	31.75
0.9	33	14.07
0.95	29	8.35

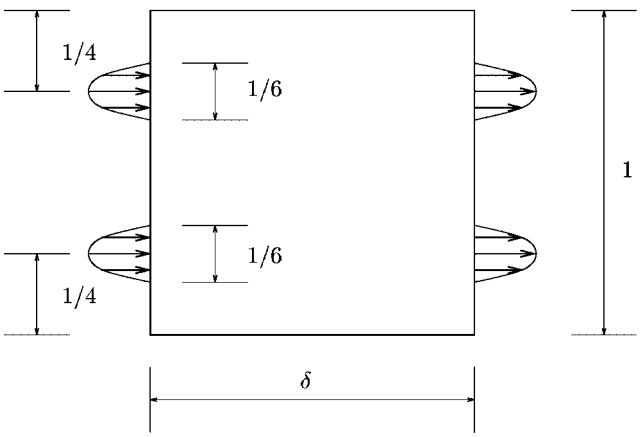

Figure 10. Design domain for the double pipe example.

problem is solved for $\delta = 1$ and $\delta = 1.5$, for which the design domain is discretized into 100×100 and 150×100 U-elements, respectively. These choices of the width-to-height ratio δ result in two solutions that are topologically different and shown in Figure 11. As for the pipe bend, the channels that transport the fluid should be short and wide and for a sufficiently large δ, it is advantageous to join the two pipes appearing in the upper solution to form the solution below. In short, there is a trade-off between transporting fluid the shortest way and to transport the fluid partly along a wide pipe in the centre of the design domain. Numerically, this problem is tricky to solve, and we find it necessary to use the solution procedure in Section 4.1 to avoid a (non-global) local optimum.

The solution at the top in Figure 11 can ideally be seen as two straight pipes that contain Stokes fluid. For such a case it is possible to compute the dissipated power analytically, a value that is equal to 32. When inspecting Table IV, which contains computational data for this example, the reader may note that the objective value for the solution at the top in Figure 11 is rather small compared to the analytically obtained dissipation value. Apart from the discretization error, there are two reasons to why this value is low. First, one may note that there is a layer of grey elements at the boundary of the pipes that allows for a decrease in the dissipated power since the 'effective' width of the pipes is larger than $\frac{1}{6}$. If needed, this effect is partly cured by choosing a larger q in (40). Secondly, some power is dissipated in the nonfluid regions because of a not-large-enough choice of $\bar{\alpha}$. From experiments, we conclude that this effect may lead to a reduction in the dissipated power with up to (and

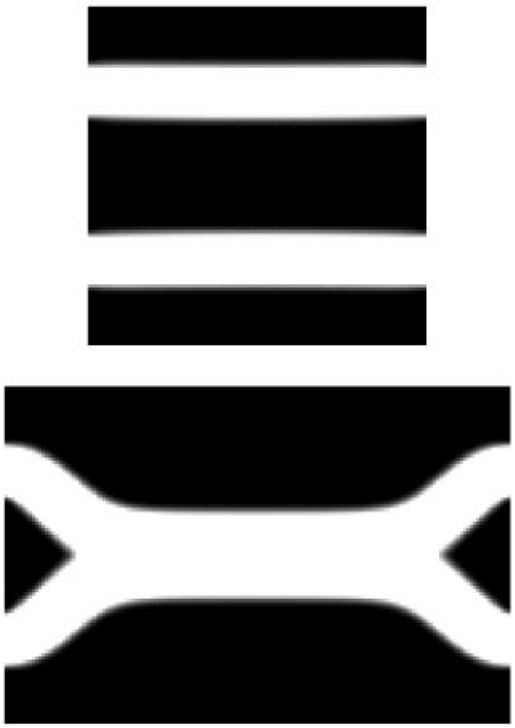

Figure 11. Optimal double pipes for $\delta = 1$ and 1.5, respectively.

Table IV. Computational data for the double pipe.

Length of domain δ	Number of iterations	Objective value
1	61	25.67
1.5	236	27.64

perhaps more than) 10%. To see if this has an effect on the optimal design, we reran the two examples in Figure 11 with values $\underline{\alpha} = 2.5\mu/1000^2$ and $\bar{\alpha} = 2.5\mu/0.001^2$ but obtained virtually identical results. It is believed that the optimal design is rather insensitive to the choice of $\bar{\alpha}$ even though the dissipated power value may deviate quite a lot from the 'true' value.

4.6. An example with a force term

We end this section with an example that includes a body fluid force term. Figure 12 shows the design domain which is discretized into 100×100 U-elements. The volume fraction is chosen $\gamma = 0.25$ and the prescribed flows on the boundary are of a magnitude defined by $\bar{g} = 1$. We have solved the problem for three horizontally directed body forces and the solutions are shown in Figure 13. For this example we also show the optimal designs including flow velocity streamlines. For the solution shown at the top, the force is directed to the left and

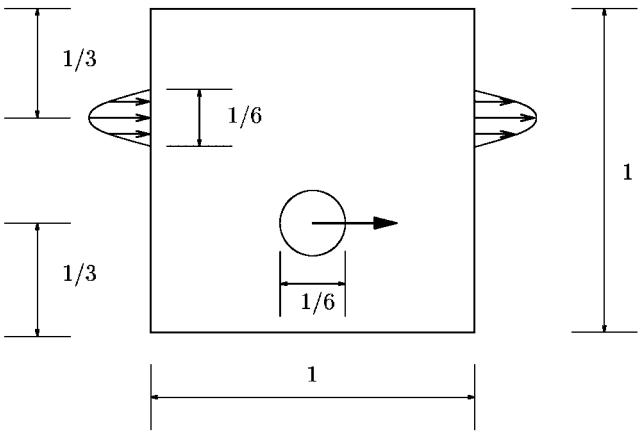

Figure 12. Design domain for the example with a force term. The circular patch on which the surface force density is defined is centred with respect to the width of the domain.

the optimal solution is a pipe that due to the force is connected to a roundabout in which the fluid flows in the clockwise direction. For a force of a certain magnitude directed to the right, the optimal design is a pipe that is shaped so that the force propels the fluid along the pipe, a situation that is illustrated by the solution shown in the middle. For this design, the incompressibility condition prevents the fluid of having a much larger velocity at the middle of the pipe than at the inlet and outlet. Consequently, a sufficiently large force to the right can be utilized more appropriately for a design shown at the bottom of the figure. Here the pipe is combined with a roundabout in which the fluid flows in the counter clockwise direction. The streamlines to the right show that the fluid velocity is approximately constant along the pipe for the design in the middle while it is higher by the applied force for the design at the bottom. Finally, we note that to obtain a successful result we had to apply the solution procedure presented in Section 4.1. Computational data for this example is found in Table V.

5. DISCUSSION AND CONCLUSIONS

A methodology for performing topology optimization of fluids in Stokes flow is presented in this paper. A generalized Stokes problem is derived from a plane flow assumption that proves to be suitable for introducing the design parameterization. Physically, the design can be seen as to control the permeability of the fluid while the viscosity is kept constant. The discretized state problem is a mixed finite element problem that is solved in the fluid pressure by a preconditioned conjugate gradient method. A preconditioner previously used in fluid mechanics applications is here slightly reformulated to handle ill-conditioning due to design oscillations, an approach that significantly improves the efficiency of the solution procedure. The optimization problem is formulated as to minimize the total potential power, which for no body fluid forces present is reduced to minimize the dissipated power in the fluid. It is shown that the optimization problem is well-posed, even if the design is required to be discrete-valued, and hence no regularization is needed. Furthermore, the finite element discretized

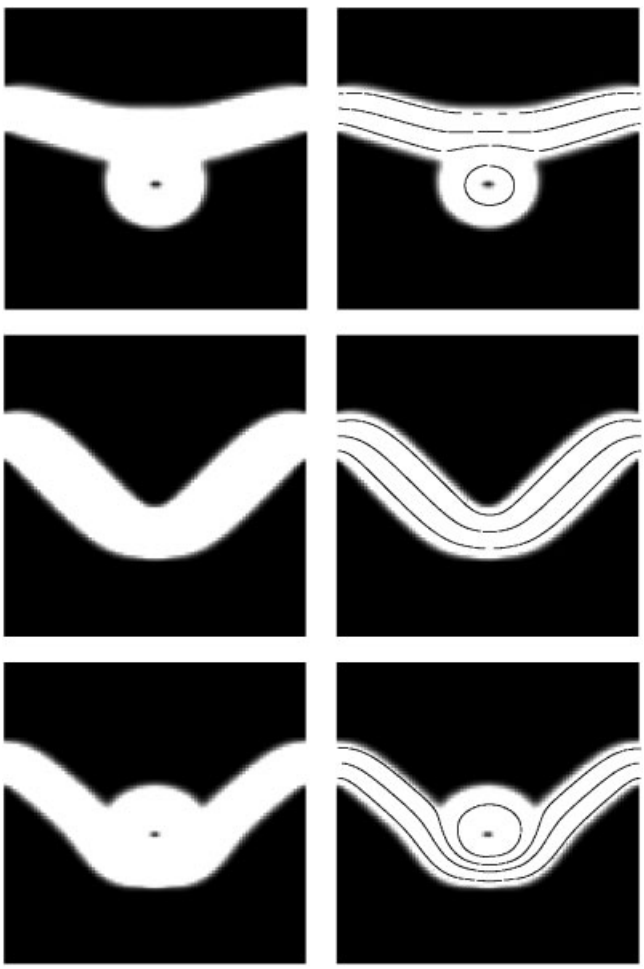

Figure 13. Optimal results for the example with a force term. The surface force density is -1125, 562.5 and 1687.5 in the direction of the arrow in Figure 12, respectively.

solutions are shown to converge to the exact ones as the mesh is infinitely refined. These results indicate that the numerical solutions are not prone to numerical instabilities, such as mesh-dependence or checkerboards, something that is also illustrated by the numerical examples. The discretized optimization problem is solved by sequential separable and convex programming, or more specifically, by MMA (the method of moving asymptotes). Several numerical examples in two dimensions are presented and compared to well-known results obtained in shape optimization of fluids.

Since the use of topology optimization methodologies in fluid mechanics seems to be new, it is not out of place to speculate about applications. First, constructions, or biological systems, involving quite slow flow on a quite small scale imply small Reynolds numbers, so the Stokes flow assumption is reasonable. One could therefore try to find applications in (integrated)

Table V. Computational data for the example with a force term. The direction of the surface force density is the one given in Figure 12.

Surface force density	Number of iterations	Objective value
−1125	229	2.19
562.5	66	−1.21
1687.5	69	−22.53

fluid circuits where the fluid paths measure about, say, less than 1 mm in width, and within biomedicine and biofluid mechanics. Second, for slow flows of quite viscous fluids such as oil, the typical length need not be very small for the Reynolds number to be small, so one could consider optimal design of fluid paths in valves.

In several of these applications the fluid device should be able to handle more than one single flow scenario. Therefore the methodology should be extended to cope with multiple boundary conditions.¶ In this paper, one should note that the properties of the optimization problem is a reason for obtaining nice mathematical results and also affects the numerical solution strategy. If an application requires usage of another objective, i.e. other than the total potential power, additional or alternative measures may need to be taken for the methodology to work satisfactory.

For some other applications that one can think of it will be necessary to include more sophisticated state equations in order to be able to govern realistic flows. One could imagine optimal conceptual design of air flow channels in vehicles, such as aircondition design for cars, as well as design of submerged bridge pillars for minimum environmental impact on watercourse flows. In such cases the Stokes model is insufficient, and one could instead try to perform optimization with e.g. the Euler equations governing inviscid flows. Then, however, it is an open question how to perform the design parameterization. Also, performing topology optimization with the Navier–Stokes equations would certainly be very desirable, but very difficult due to the careful resolution that is needed close to the unknown boundaries.

APPENDIX A: INTERPRETATION OF $\phi(\rho)$ AS AVERAGE PRESSURE DROP

We return to the three-dimensional continuum mechanical description initiated in Section 2.1, and consider cases when $\bar{\boldsymbol{f}} = \boldsymbol{0}$ and $\bar{\boldsymbol{g}} = \bar{g}\boldsymbol{n}$.

We start by making the following observation. Denoting the surface traction by $\boldsymbol{s}(\boldsymbol{n})$, on $\partial\mathscr{R}$ it holds that

$$\boldsymbol{s}(\boldsymbol{n}) \cdot \bar{\boldsymbol{u}} = -\bar{p}(\bar{\boldsymbol{g}} \cdot \boldsymbol{n}) + 2\mu \boldsymbol{D}(\bar{\boldsymbol{u}})\boldsymbol{n} \cdot \bar{\boldsymbol{u}}$$

due to $\boldsymbol{s}(\boldsymbol{n}) = \boldsymbol{T}\boldsymbol{n}$ (Cauchy's theorem) and the constitutive equation (1). Using (2) this can be rewritten as

$$\boldsymbol{s}(\boldsymbol{n}) \cdot \bar{\boldsymbol{u}} = -\bar{p}(\bar{\boldsymbol{g}} \cdot \boldsymbol{n}) + \mu(\nabla \bar{\boldsymbol{u}})\bar{\boldsymbol{u}} \cdot \boldsymbol{n} + \mu(\nabla \bar{\boldsymbol{u}})\boldsymbol{n} \cdot \bar{\boldsymbol{u}}$$

¶This is analogous to multiple loads in solid mechanics and should not provide any principal complications.

and in particular, when $\bar{\boldsymbol{g}} = \bar{g}\boldsymbol{n}$ and neglecting the convection terms,

$$\boldsymbol{s}(\boldsymbol{n}) \cdot \bar{\boldsymbol{g}} \approx -\overline{pg} \tag{A1}$$

For the three-dimensional case we can identify the multiplier $\lambda(\rho)$ with the surface traction $\boldsymbol{s}(\boldsymbol{n})$, so by (A1) and (31) one gets that

$$\phi(\rho) \approx -\frac{1}{2}\int_{\partial\mathscr{R}} \overline{pg}$$

so the objective is to maximize $\int_{\partial\mathscr{R}} \overline{pg}$. Define $\partial\mathscr{R}_{\text{in}}$ as the part of $\partial\mathscr{R}$ where $\bar{g} < 0$ and $\partial\mathscr{R}_{\text{out}}$ the part of $\partial\mathscr{R}$ where $\bar{g} > 0$, and then define the average pressures

$$\bar{p}_{\text{in}} = \frac{\int_{\partial\mathscr{R}_{\text{in}}} \overline{g\,p}}{\int_{\partial\mathscr{R}_{\text{in}}} \bar{g}}, \quad \bar{p}_{\text{out}} = \frac{\int_{\partial\mathscr{R}_{\text{out}}} \overline{g\,p}}{\int_{\partial\mathscr{R}_{\text{out}}} \bar{g}}$$

From the compatibility condition (6) one has

$$-\int_{\partial\mathscr{R}_{\text{in}}} \bar{g} = \int_{\partial\mathscr{R}_{\text{out}}} \bar{g} > 0$$

so

$$\begin{aligned}\phi(\rho) \approx -\frac{1}{2}\int_{\partial\mathscr{R}} \overline{pg} &= \frac{1}{2}\left(\frac{\int_{\partial\mathscr{R}_{\text{in}}} \overline{g\,p}}{\int_{\partial\mathscr{R}_{\text{in}}} \bar{g}} - \frac{\int_{\partial\mathscr{R}_{\text{out}}} \overline{g\,p}}{\int_{\partial\mathscr{R}_{\text{out}}} \bar{g}}\right)\int_{\partial\mathscr{R}_{\text{out}}} \bar{g} \\ &= \frac{1}{2}(\bar{p}_{\text{in}} - \bar{p}_{\text{out}})\int_{\partial\mathscr{R}_{\text{out}}} \bar{g}\end{aligned}$$

Therefore, since the flow $\int_{\partial\mathscr{R}_{\text{out}}} \bar{g}$ through the control volume is given, the design goal in this common special case is to

$$\text{minimize } (\bar{p}_{\text{in}} - \bar{p}_{\text{out}})$$

In conclusion, neglecting similar nonlinear terms as when deriving Stokes equations from Navier–Stokes equations, and assuming $\bar{\boldsymbol{g}} = \bar{g}\boldsymbol{n}$, $\bar{\boldsymbol{f}} = \boldsymbol{0}$, the chosen design objective (31) means to *minimize the average pressure drop*.

ACKNOWLEDGEMENTS

This work was financially supported by the National Graduate School in Scientific Computing (NGSSC) and National Network in Applied Mathematics (NTM) up to and including the year 2001. After that the support comes from the Swedish Research Council (VR) and the Center for Industrial Information Technology (CENIIT).

The authors wish to express their gratitude to Martin Berggren, Department of Scientific Computing, Uppsala University, and FOI, Swedish Defence Research Agency, Stockholm, for his invaluable help on the Stokes problem solver. Further, Joakim Wren, Department of Mechanical Engineering, Linköping university, and Matts Karlsson, Department of Biomedical Engineering, Linköping university, are acknowledged for their suggestions on the numerical examples.

REFERENCES

1. Enoksson O. Shape optimization in compressible inviscid flow. *Licentiate thesis* LiU-TEK-LIC-2000:31, Department of Mathematics, Linköpings Universitet, 2000.
2. Kim DW, Kim, M-U. Minimum drag shape in two-dimensional viscous flow. *International Journal for Numerical Methods in Fluids* 1995; **21**:93–111.
3. Pironneau O. On optimum profiles in Stokes flow. *Journal of Fluid Mechanics* 1973; **59**:117–128.
4. Pironneau O. On optimum design in fluid mechanics. *Journal of Fluid Mechanics* 1974; **64**:97–110.
5. Glowinski R, Pironneau O. On the numerical computation of the minimum-drag profile in laminar flow. *Journal of Fluid Mechanics* 1975; **72**:385–389.
6. Çabuk H, Modi V. Optimum plane diffusers in laminar flow. *Journal of Fluid Mechanics* 1992; **237**:373–393.
7. Bendsøe MP. *Optimization of Structural Topology*, *Shape*, *and Material*. Springer-Verlag: Berlin, 1995.
8. Eschenauer HA, Olhoff N. Topology optimization of continuum structures: A review. *Applied Mechanics Review* 2001; **54**:331–390.
9. Karlsson M, Klarbring A, Petersson J, Torstenfelt B. Topology optimization of flow networks. In preparation.
10. Bendsøe MP, Sigmund O. Material interpolation schemes in topology optimization. *Archives of Applied Mechanics* 1999; **69**:635–654.
11. Cahouet J, Chabard JP. Some fast 3D solvers for the generalized Stokes problem. *International Journal for Numerical Methods in Fluids* 1988; **8**:269–295.
12. Glowinski R. Finite element methods for the numerical simulation of incompressible viscous flow: Introduction to the control of the Navier–Stokes equations. *Lectures in Applied Mathematics* 1991; **28**:219–301.
13. Sanchez-Palencia E. *Non-Homogeneous Media and Vibration Theory*. Springer-Verlag: Berlin, Heidelberg, 1980.
14. Gurtin ME. *An Introduction to Continuum Mechanics*. Academic Press: San Diego, 1981.
15. Girault V, Raviart P. *Finite Element Methods for Navier–Stokes Equations*: *Theory and Algorithms*. Springer-Verlag: Berlin, Heidelberg, 1986.
16. Brezzi F. On the existence, uniqueness and approximation of saddle point problems arising from Lagrangian multipliers. *RAIRO Numerical Analysis* 1974; **8**:129–151.
17. Glowinski R. *Numerical Methods for Nonlinear Variational Problems*. Springer Verlag: Berlin, 1984.
18. Ekeland I, Temam R. *Convex Analysis and Variational Problems*. North-Holland: Amsterdam, 1976.
19. Ciarlet PG. *The Finite Element Method for Elliptic Problems*. North-Holland: Amsterdam, 1978.
20. Petersson J. A finite element analysis of optimal variable thickness sheets. *SIAM Journal for Numerical Analysis* 1999; **36**:1759–1778.
21. Svanberg K. The method of moving asymptotes—a new method for structural optimization. *International Journal for Numerical Methods in Engineering* 1987; **24**:359–373.
22. Clarke FH. *Optimization and Nonsmooth Analysis*. John Wiley: New York, 1983.

